Neuron

Article

Axon morphogenesis and maintenance require an evolutionary conserved safeguard function of Wnk kinases antagonizing Sarm and Axed

Highlights

- Wnk kinases regulate axon branching in fly neurons and mouse cortical pyramidal neurons
- Independently, dWnk and WNK1/2 are also constitutively required in adult axon maintenance
- dWnk positively supports Nmnat function and suppresses D-Sarm and Axundead
- Wnk regulates a conserved network linking axon branching, maintenance, and degeneration

Authors

Azadeh Izadifar, Julien Courchet, Daniel M. Virga, ..., Tommy Lewis, Franck Polleux, Dietmar Schmucker

Correspondence

julien.courchet@univ-lyon1.fr (J.C.), fp2304@columbia.edu (F.P.), dslab@uni-bonn.de (D.S.)

In brief

Izadifar, Courchet, et al. demonstrate an evolutionary conserved role for Wnk kinases in axon morphogenesis and adult axon maintenance. These dual roles of Wnk kinases involve regulation of components of the Wallerian degeneration network. This study provides evidence for a shared regulatory network linking developmental axon branching, maintenance, and degeneration.

Izadifar et al., 2021, Neuron *109*, 2864–2883
September 15, 2021
https://doi.org/10.1016/j.neuron.2021.07.006

CellPress

CellPress

Neuron

Article

Axon morphogenesis and maintenance require an evolutionary conserved safeguard function of Wnk kinases antagonizing Sarm and Axed

Azadeh Izadifar,[1,2,3,9] Julien Courchet,[4,5,9,*] Daniel M. Virga,[5] Tine Verreet,[2,3] Stevie Hamilton,[5] Derya Ayaz,[2,3] Anke Misbaer,[2,3] Sofie Vandenbogaerde,[2,3] Laloe Monteiro,[4] Milan Petrovic,[2,3] Sonja Sachse,[2,3] Bing Yan,[2,3] Maria-Luise Erfurth,[2,3] Dan Dascenco,[2,3] Yoshiaki Kise,[7] Jiekun Yan,[2,3] Gabriela Edwards-Faret,[1,2,3] Tommy Lewis,[5,8] Franck Polleux,[5,6,*] and Dietmar Schmucker[1,2,3,10,*]

[1]Life and Medical Sciences Institute (LIMES), Bonn, Germany
[2]VIB Center for Brain & Disease Research, Leuven, Belgium
[3]Department of Neurosciences, KU Leuven, Leuven, Belgium
[4]Univ Lyon, Université Claude Bernard Lyon 1, CNRS UMR-5310, INSERM U-1217, Institut NeuroMyoGène, 69622 Villeurbanne, France
[5]Department of Neuroscience, Mortimer B. Zuckerman Mind Brain Behavior Institute, Columbia University, New York, NY, USA
[6]Kavli Institute for Brain Science, Columbia University, New York, NY, USA
[7]University of Tokyo, Tokyo, Japan
[8]Aging & Metabolism Program, Oklahoma Medical Research Foundation, Oklahoma City, OK, USA
[9]These authors contributed equally
[10]Lead contact
*Correspondence: julien.courchet@univ-lyon1.fr (J.C.), fp2304@columbia.edu (F.P.), dslab@uni-bonn.de (D.S.)
https://doi.org/10.1016/j.neuron.2021.07.006

SUMMARY

The molecular and cellular mechanisms underlying complex axon morphogenesis are still poorly understood. We report a novel, evolutionary conserved function for the *Drosophila* Wnk kinase (dWnk) and its mammalian orthologs, WNK1 and 2, in axon branching. We uncover that dWnk, together with the neuroprotective factor Nmnat, antagonizes the axon-destabilizing factors D-Sarm and Axundead (Axed) during axon branch growth, revealing a developmental function for these proteins. Overexpression of D-Sarm or Axed results in axon branching defects, which can be blocked by overexpression of dWnk or Nmnat. Surprisingly, Wnk kinases are also required for axon maintenance of adult *Drosophila* and mouse cortical pyramidal neurons. Requirement of Wnk for axon maintenance is independent of its developmental function. Inactivation of dWnk or mouse Wnk1/2 in mature neurons leads to axon degeneration in the adult brain. Therefore, Wnk kinases are novel signaling components that provide a safeguard function in both developing and adult axons.

INTRODUCTION

A hallmark in the generation of neuronal cell type diversity is the acquisition of diverse morphologies, which requires the formation of axonal and dendritic compartments ranging from simple to highly complex, depending on the degree of neurite branching. Specifying the degree and pattern of neurite branching is crucial in brain development, as it directly impacts the total number and spatial distribution of synaptic contacts of each circuit element (Courchet et al., 2013; Iascone et al., 2020; Chia et al., 2014; Urwyler et al., 2019). However, the identity of the molecular effectors determining how diverse, cell-type-specific patterns of axon arborization are established and how they are stabilized as well as maintained throughout the life of an organism remains a major challenge (Südhof, 2017).

We performed a reverse genetic screen to identify novel regulators of axon branching by utilizing an experimental system in *Drosophila* that combines efficient single-neuron labeling and simultaneous knockdown of candidate genes (Urwyler et al., 2019). Clear orthologs of selective candidates were then further examined in vertebrates. Using this approach, we found that loss of the *Drosophila* dWnk kinase specifically disrupts axon growth and branch patterning of mechanosensory neurons. Surprisingly, unlike other essential regulators of axon branching (Sudarsanam et al., 2020; He et al., 2014; Dascenco et al., 2015; Lewis et al., 2013), we discovered that dWnk is also continuously required in mature neurons for axon maintenance. Moreover, comparative studies in mouse cortical pyramidal neurons (PNs) provide strong evidence that both of these functions of Wnk kinases are conserved and required in PNs, i.e., long-range projecting mammalian neurons of the central nervous system (CNS).

Wnk kinases are present in most multicellular organisms, including plants and some unicellular organisms, but not in yeast

(Hoorn et al., 2011; McCormick and Ellison, 2011). Mammals have four Wnk kinases (WNK1–4) and *Drosophila* one (dWnk). The WNK ("with no K(lysine)") kinases are catalytically active but are referred to as "atypical kinases" because a catalytically important lysine residue is swapped from subdomain II to subdomain I (Xu et al., 2000; Veríssimo and Jordan, 2001). WNK proteins are involved in a broad spectrum of diseases (e.g., hypertension, sensory and autonomic neuropathy, osteoporosis, and many different cancers; McCormick and Ellison, 2011; Alessi et al., 2014; Siew and O'Shaughnessy, 2013; Sato and Shibuya, 2018).

The majority of studies on human WNK kinases have been conducted in the context of blood pressure regulation, due to the identification of mutations in human patients with hereditary hypertension (familial hyperkalemia and hypertension [FHHt] or Gordon's syndrome; Wilson et al., 2001). For this reason, a major focus in dissecting WNK function has been on studying renal regulation of ion transport (Alessi et al., 2014; Yang et al., 2003; Pela, 2012; Vidal-Petiot et al., 2013; Jun et al., 2009; Costa et al., 2015). However, regulation of ion homeostasis is only one of multiple functions of WNK kinases (Siew and O'Shaughnessy, 2013; Gallolu et al., 2018), and they are broadly expressed, including in the developing as well as mature brain. In rare cases, WNK function has been linked to a severe form of peripheral sensory neuropathy (hereditary sensory and autonomic neuropathy type 2, HSNA2; Lafreniere et al., 2004; Rivière et al., 2004; Roddier et al., 2005; Coen et al., 2006); however, their developmental, cellular, and molecular mechanisms are poorly understood in neurons. The fact, however, that most identified mutations cluster in a neuron-specific alternatively spliced exon (HSN2) of human Wnk1 supports the notion that Wnk1 kinase plays an important role in sensory neurons (Shekarabi et al., 2008; Yuan et al., 2017; Rahmani et al., 2018).

In the process of studying the role of dWnk kinase in fly sensory neurons, we identified novel interactors of Wnk kinases. Specifically, we found that nicotinamide mononucleotide adenylyltransferase (Nmnat), Sarm, and Axundead (Axed) are molecular interactors of dWnk. While Nmnat is broadly required for axon maintenance, Sarm and Axed are primarily studied for their roles as effectors in active axon degeneration (e.g., in Wallerian degeneration) in response to axon injury (Coleman and Freeman, 2010; Gilley and Coleman, 2010; Neukomm et al., 2017; Osterloh et al., 2012). We provide evidence that dWnk and Nmnat have synergistic functions in axon growth and branching but are also required in post-developmental processes to continuously support axon maintenance. The function of dWnk is evolutionarily conserved, as their mouse orthologs WNK1 and WNK2 are both required in cortical PNs during axon morphogenesis as well as maintenance. Genetic epistasis analysis demonstrates that both dWnk and Nmnat functions during axon development and axon maintenance are mediated by antagonizing the axon destruction function of Sarm and Axed. Depletion of axon-protective factors (e.g., dWnk/WNK1/2 and Nmnat) during development leads to axon branching defects, whereas their depletion in mature neurons eliminates their safeguard function and initiates spontaneous axon degeneration in the absence of axon injury.

RESULTS

Wnk is required for axonal branch patterning in fly mechanosensory neurons

To identify signaling factors regulating axon branching during CNS development, we focused on the central projections of *Drosophila* mechanosensory neurons that innervate sensory bristles of the adult fly thorax (Figures 1A and 1B). Mechanosensory neurons from the central domain of the thorax all extend axonal projections to the ventral nerve cord (VNC), where they establish a cell-type-specific and stereotyped axonal branching pattern (Chen et al., 2006). Single-cell labeling using either lipophilic dye fills (Chen et al., 2006) or genetic mosaic labeling (He et al., 2014; Urwyler et al., 2015) allows the visualization of the precise axonal branching pattern within the VNC (Figures 1B and 1D).

In a reverse genetic screen, we examined the potential role of the majority of *Drosophila* kinases as well as phosphatases (Dascenco et al., 2015) and found that RNAi-mediated knockdown of *Drosophila* Wnk kinase (dWnk) leads to a rather unique phenotype characterized by strong impairment of axonal branching of many mechanosensory axon projections (Figures 1B and 1C). Specifically, knockdown of dWnk in posterior scutellar (pSC) mechanosensory neurons strongly impaired axon collateral formation and patterning within the *Drosophila* CNS (Figures 1D–1F). In mutant axons, extensions of collaterals along the long posterior and contralateral projections were almost absent. Instead, a plexus of unpatterned and seemingly randomly projecting short axon branches were formed (Figures 1E and 1F).

We next examined two dWnk loss-of-function (LOF) alleles (Wnk^{G1286} and Wnk^{F1183}) using mosaic analysis with a repressible cell marker (MARCM). These LOF alleles harbor ethyl methanesulfonate-induced point mutations, resulting in strong (Wnk^{G1286}) or complete (Wnk^{F1183}) LOF (Figure S1), and have previously been characterized (Berger et al., 2008). Anti-Wnk antibodies show that dWnk is broadly expressed throughout the nervous system (Figures S1D–S1F and S2A–S2D) and absent in homozygous Wnk^{F1183} animals (Figures S1B–S1G). Immunostaining reveals that endogenous dWnk protein localizes to the cytoplasm and also throughout axonal processes, including growth cones (Figures S2E–S2H). Single-cell labeling in both homozygous mutant pSc neurons (Figures 1G and 1H) revealed qualitatively similar axon branching defects as found by RNAi-mediated knockdown of dWnk (Figures 1E and 1F). These defects were substantially rescued cell autonomously by overexpression of *dWnk* cDNA in mechanosensory neurons (Figure 1I). Moreover, an analogous analysis of a functionally similar yet different mechanosensory neuron, the posterior dorsocentral neuron (pDc) (Figure 1A), revealed similar defects of axon branching as found in pSc neurons (Figures 1J–1M). Moreover, analysis of other neuron types using knockdown or LOF alleles revealed a strong requirement of dWnk in olfactory sensory neurons with defects in axon growth, branching, and targeting (Figures S3A–S3F). In addition to these requirements in sensory neurons, dWnk is also required in interneurons of the visual system (DCN; Figures S3G and S3H). Analysis of dorsal cluster neurons (DCN) neurons suggests the possibility that dWnk is primarily important for axon branch extension within the target area, but not in growth or branching of the dendritic compartment. Analysis of MARCM clones of DCN neurons

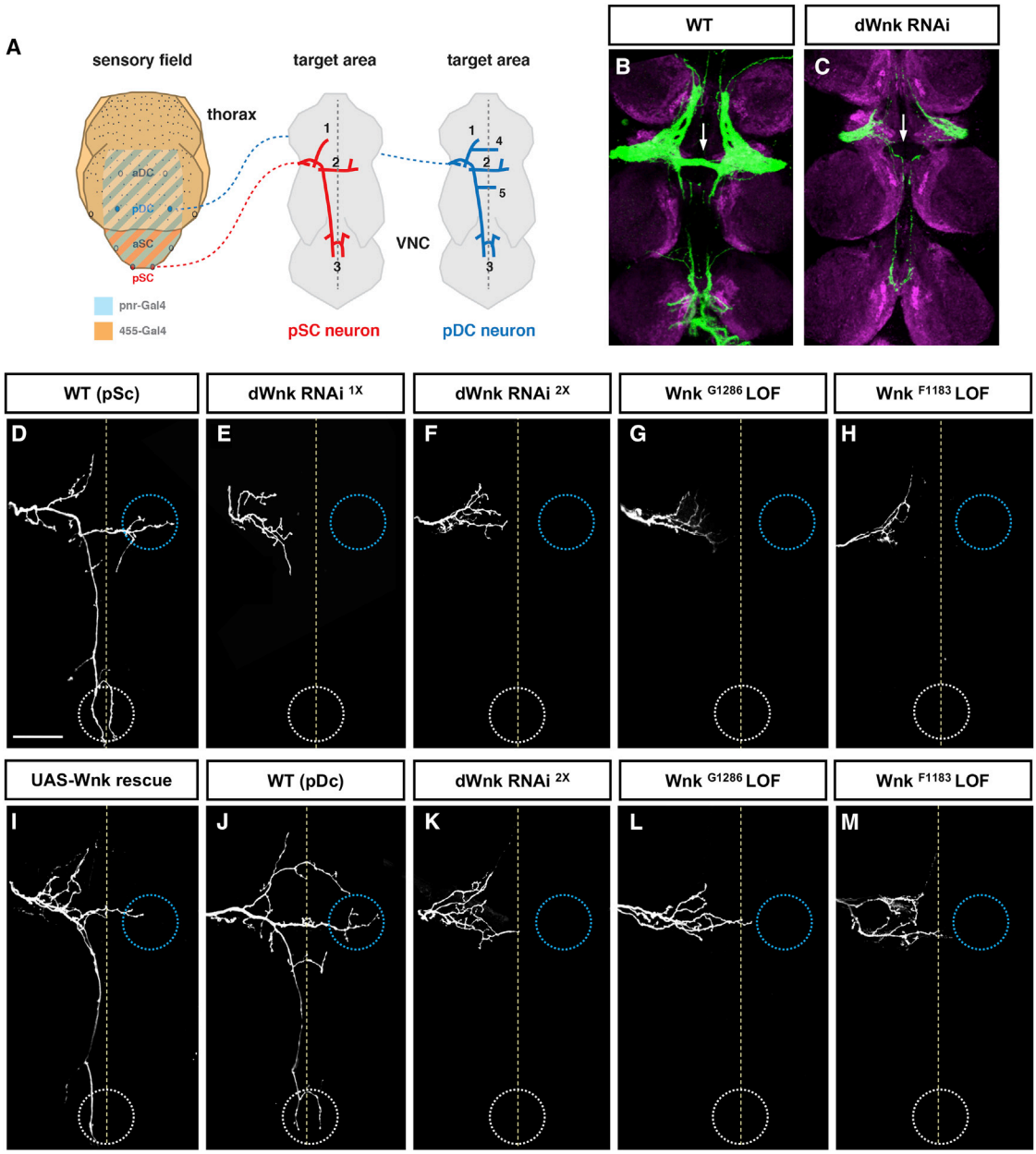

Figure 1. Loss of *Drosophila* dWnk results in axon branching defects in mechanosensory neurons

(A) Stereotyped branching pattern of *Drosophila* mechanosensory neurons.

(B and C) GFP-labeled population of mechanosensory axons within the anterior part of the VNC. Note the complete lack of commissure (white arrows) in dWnk RNAi knockdown.

(D–M) Representative confocal images of mechanosensory neurons dye filled with carbocyanine dyes.

(D and J) Wild-type (WT) pSc and pDc mechanosensory neurons displaying the stereotyped branching pattern.

(E, F, and K) dWnk RNAi and double RNAi ($RNAi^{2\times}$)-mediated knockdown defects result in branching defects.

(I) Overexpression of dWnk can rescue branching defects in dWnk LOF.

(G, H, L, and M) dWnk LOF phenotypes using MARCM clones of two dWnk alleles, Wnk^{G1286} and Wnk^{F1183}, also lead to defects in axon branch growth and patterning.

Scale bar: 20 μm.

in adult flies (Figures S3I and S3J) as well as clones of dorsal arborization neurons (ddaE-class I sensory neurons) in larvae did not reveal any defects in dendrite patterning of these neurons (Figures S3K and S3L). Taken together, this suggests a cell-autonomous requirement of *Drosophila Wnk* in multiple sensory and interneuron types and that this function is specific to axon morphogenesis.

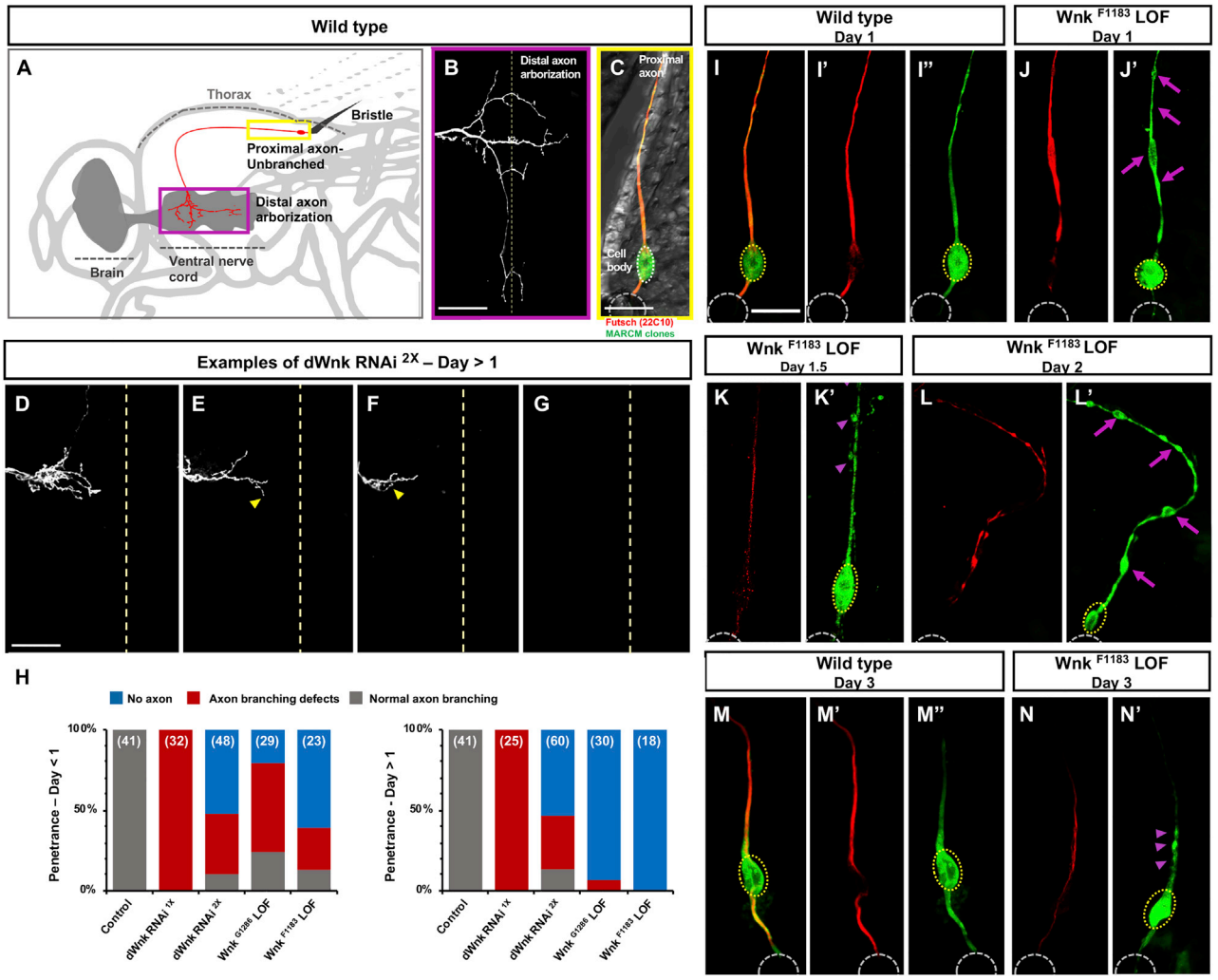

Figure 2. Loss of *Drosophila* dWnk function causes early-onset neurodegeneration in mature sensory neurons and progressive loss of axons on thorax

(A) Schematic of *Drosophila* thorax showing the location of the scutellar mechanosensory neurons (in red) with a part of the proximal axon, cell body, dendrite (yellow box), and a distal axon in the ventral nerve cord (magenta box).

(B) Magnified image of distal axon showing arborization of mechanosensory neurons.

(C) A part of scutellum of adult *Drosophila* thorax (in gray) with anti-22C10 (microtubule binding protein) staining labeling of mechanosensory neuron (here, pSc neurons). 22C10 labels microtubules in red and the CD8-GFP labeling axon membrane in green (C and I–O).

(D–G) Representative confocal images of mechanosensory neurons dye filled with carbocyanine dyes. Loss of axon terminals in *Drosophila* mechanosensory neurons between 1 and 3 days in dWnk LOF is shown. The axon degeneration in loss of dWnk knockdown neurons starts at day 1 (D), followed by degeneration of distal axons (E and F), and resulted in loss of axons in 3-day-old samples (G).

(H) Quantification of the total number of degenerating axons in RNAi-mediated knockdown of dWnk (one copy and two copies) and two different Wnk alleles ($WnkG^{1286}$ and $WnkF^{1183}$) at two developmental stages, 1 day and 3 days.

(I–O) Process of axon degeneration in WT (I) and (M) and dWnk homozygous mutant neurons using MARCM (J–L and N) in different developmental stages.

(J and L) Genetic mosaic analysis shows that loss of dWnk leads to axon swelling and blebbing (arrows in magenta). Then, the axon starts to undergo fragmentation (arrow heads in magenta; K), followed by complete fragmentation and clearance of axonal debris (N).

Scale bar: 20 μm.

Loss of dWnk in mechanosensory neurons leads to early-onset axon degeneration in adult flies

The phenotypic effects on axon branching characterizing dWnk RNAi knockdown or MARCM clones for strong LOF alleles were similar (Figures 1C, 1E–1H, and 1K–1M). However, we noted that many samples of flies with Wnk^{G1286} or Wnk^{F1183} mutant mechanosensory neurons and in particular samples older than 2 days (post-eclosion) had no axonal projections within the VNC target area (Figure 2).

We therefore determined quantitatively the number of samples where mutant axons had reached the VNC in adult flies at different time points post-eclosion (Figures 2D–2H). Within the

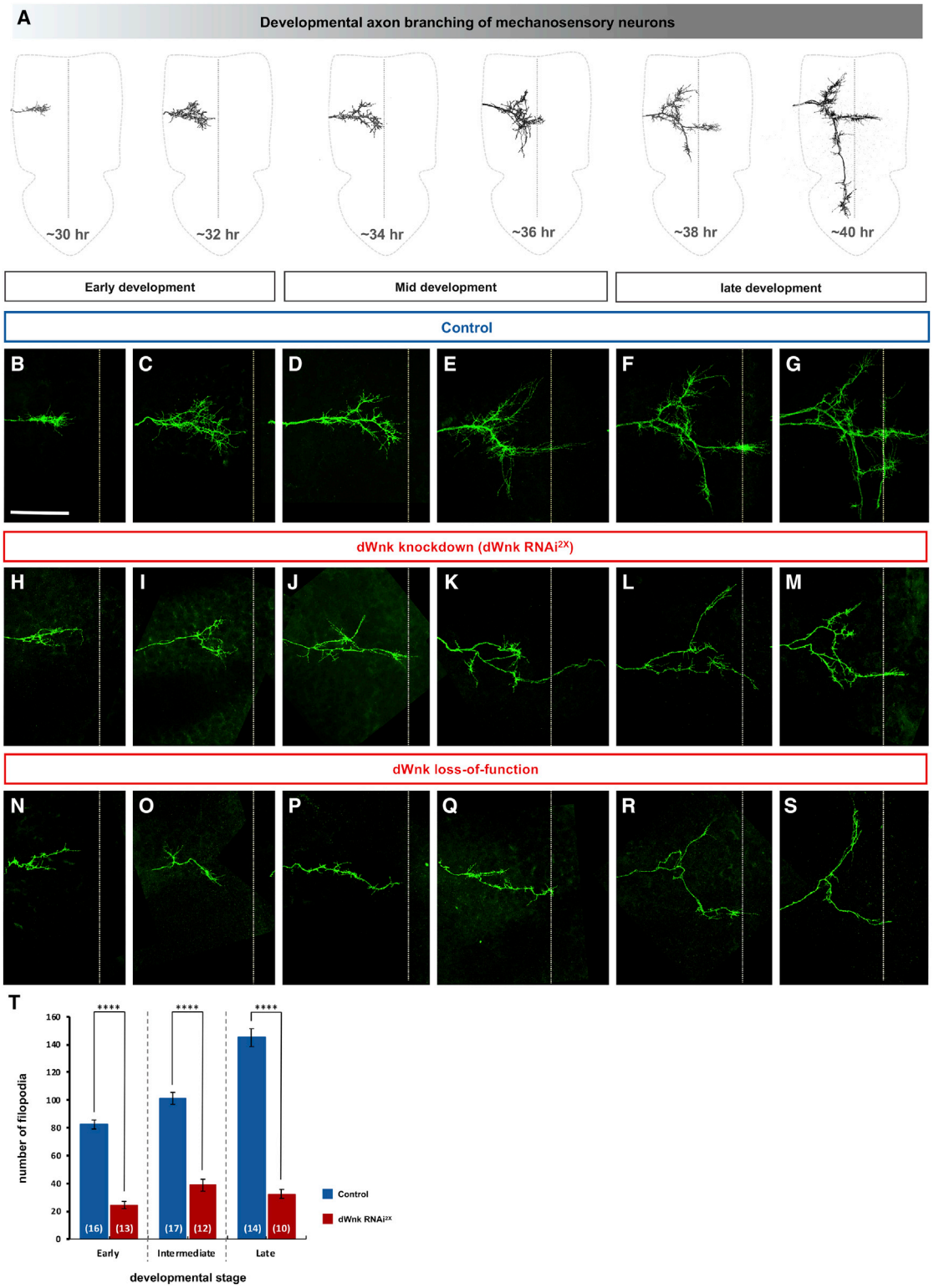

Figure 3. dWnk is required for developmental axon branching

(A) Schematic of a *Drosophila* mechanosensory neuron development.

(A–C) During early development, WT pDC neurons growth cones enter the CNS at ~30 h APF (after puparium formation) and undergo extensive expansion at ~32 h APF.

(legend continued on next page)

first 24 h (<day 1) after eclosion, ~40% of Wnk^{F1183} and ~80% of Wnk^{G1286} mutant neurons still had central axonal projections in the VNC. In all samples where an axon was present in the VNC target area, we observed strong axon branching defects similar to the RNAi knockdown samples (Figures 2D–2F). In older adult flies, however, no axon or only traces of remaining axon branches were detectable in Wnk^{F1183} mutant neurons and very few in Wnk^{G1286} mutant neurons (Figures 2G and 2H), suggesting a progressive loss of axons over time.

In contrast, either at day 1 or in older flies, we never observed a loss of axons in the VNC of flies expressing a single copy of upstream activating sequence (UAS)-dWnk RNAi (dWnk $RNAi^{1\times}$), despite strong and highly penetrant axon branching defects (Figure 1E; left panel of Figure 2H). Therefore, we examined whether enhancing the RNAi-mediated knockdown of dWnk would initiate degeneration. Indeed, using two copies of UAS-dWnk RNAi (dWnk $RNAi^{2\times}$) did lead to a 50% reduction of distal axons in the respective samples compared to controls or single-copy UAS-dWnk RNAi (Figure 2H). These results suggest a dose dependence of dWnk expression for proper axon maintenance in mechanosensory neurons. However, the axon branching defects displayed little phenotypic variability because they were observed in all RNAi or LOF alleles examined (see above; Figure 1 and left panel of Figure 2H). In contrast, the degeneration following the loss of dWnk function showed significant allelic differences; appeared to be progressive; and, only in mutants carrying the strongest loss of dWnk allele, all axons had degenerated in 3 days or older flies (Figure 2H).

To better characterize the progressive nature of the axon degeneration phenotype due to dWnk LOF, we took advantage of the fact that we could visualize and identify the proximal part of the main axon (unbranched axon) close to the cell body (Figures 2A and 2C) through the thin cuticle of the thorax by using single-neuron GFP expression and antibody-based detection of microtubule organization (using anti-22C10 antibody against Futsch, a microtubule-associated protein in *Drosophila* neurons; Figure 2C). We examined wild-type and dWnk mutant neurons (dendrite, soma, and axon) in the scutellar part of adult flies (Figures 2I–2N).

We detected a near continuous labeling of the axon and microtubule cytoskeleton using membrane-tethered CD8-GFP and anti-22C10 antibody staining in wild-type control samples (Figures 2I and 2M). In contrast, dWnk mutant neurons showed moderate signs of axonal degeneration already in 1-day-old flies (Figure 2J). In particular, in mutant neurons with strong dWnk LOF, the severity of axonal defects correlated with the age of the flies (Figures 2L and 2N). In 3-day-old mutant neurons, we often detected only segments of the most proximal axon and membrane blebbing or loss of cytoskeletal integrity were prominent (Figure 2N). These results provide evidence that loss of dWnk in mechanosensory neurons triggers progressive and spontaneous axon degeneration.

It seems plausible that the distal axon branching defects within the VNC lead directly to axon degeneration, possibly as a consequence of losing target-derived trophic support once these mechanosensory axons reached the CNS.

Nevertheless, to test more directly an adult-specific requirement for axon maintenance, we induced RNAi-dependent knockdown of dWnk following the completion of axon branching at the end of pupal stages (Figures S4A and S4B). We used temperature shifts to control the timing of RNAi expression such that dWnk expression is either absent during larval and early pupal stages, which reproduced the axon branching followed by axon degeneration as shown above (Figures S4B–S4E), or present during the developmental phase of axon growth and branching but absent starting at late pupal and adult stages (Figures S4B, S4C, S4F, and S4G). Indeed, the latter manipulation, i.e., a late knockdown of dWnk, did not disrupt the axon branch patterning at early stages (Figures S4B, S4C, and S4F) but clearly triggered axon degeneration of adult mechanosensory neurons 3–5 days after hatching (Figure S4G). This temporal dissection of dWnk knockdown supports the model of a requirement of adult expression of dWnk for axon maintenance, independent of its role in axon development.

In summary, dWnk mutant mechanosensory axons can grow from the periphery to the VNC but require dWnk function during axonal branch growth and patterning of its arborization in the VNC target area.

Loss of dWnk impairs axonal branch extension and stabilization during early developmental stages

In order to better characterize the role of dWnk during axon morphogenesis, we analyzed axon growth at multiple time points (2-h time windows) during pupal development (Figure 3A). In wild-type animals, axon extension into the VNC is completed before 30 h of pupal development. At this time point, unpatterned axon sprouting is initiated. Subsequent branch extensions, consolidation, and selective primary collateral formation proceed within the next 10 h (Figures 3A–3G). In contrast, Wnk knockdown (Wnk $RNAi^{2\times}$; Figures 3H–3M) or Wnk mutants axons (Wnk LOF; Figures 3N–3S) show an abnormal axon

(A and D) During the intermediate phases, the growth cones composed of filopodia-like extension start to expand and sprout into all directions at ~34 h APF.
(A and E) The number and length of filopodia are dramatically increased and segregated in opposite directions, along the anterior-posterior axis as well as toward the midline at ~36 h APF.
(A and F) In late development, the main axon shaft is growing in length and the midline projecting axon becomes more prominent and grows contralaterally ~38 h.
(A and G) This process is sustained until the neurons reach their final length at ~40 h APF, after which the axon matures and stabilizes its branching pattern.
(H–M) Growth cones of Dc neurons with dWnk double RNAi knockdown and Wnk LOF (N–S) are highly abnormal, exhibiting a reduced number of filopodia-like extensions. During the entire time course, Wnk mutant axons are not capable of executing a normal axonal branching program.
(H–S) Even starting from the earliest time points of axonal sprouting (~30–32 h APF), the erroneous growth of axon collaterals, as well as strong deficits in spatial patterning of axon collaterals, persists into later stages (~30–32 h APF).
(T) Quantification of the total number of filopodia at different developmental stages in control and Wnk mutant in animals of the genotypes indicated in (B)–(M). The tests were considered significant when $p < 0.05$, with the following criteria: *$p < 0.05$; **$p < 0.01$; ***$p < 0.001$; and ****$p < 0.0001$; ordinary one-way ANOVA with multiple comparisons.
Scale bar: 20 μm.

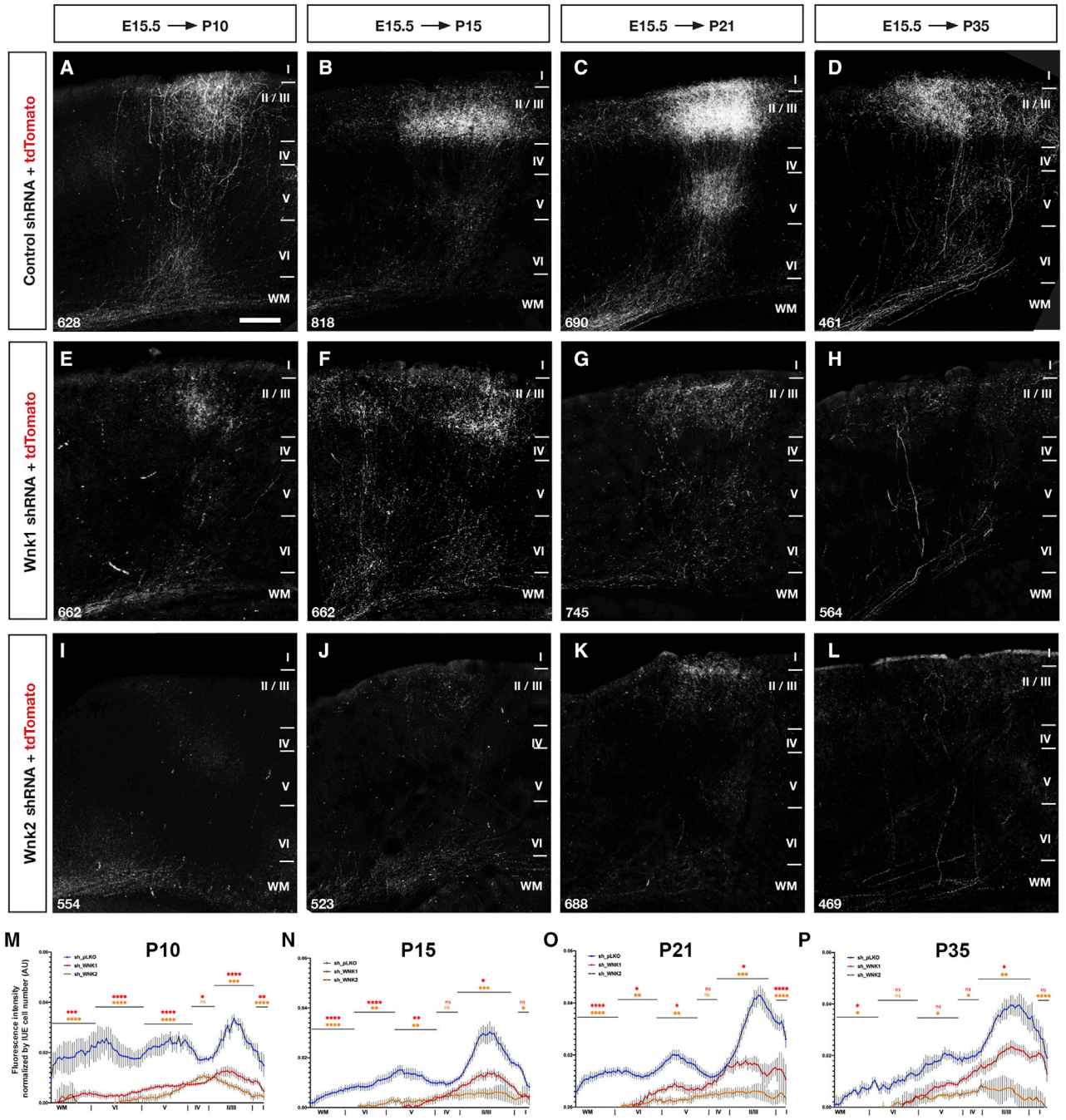

Figure 4. Wnk1 and Wnk2 are both required for terminal axon branching and maintenance *in vivo*

(A–L) Representative images of the axons on the contralateral side of the electroporation in layer 2/3 PNs co-electroporated with tdTomato and control shRNA (A–D) or *Wnk1* shRNA expressing (E–H) or *Wnk2* shRNA (I–L). *In utero* cortical electroporation (IUCE) was performed at E15 to electroporate neural progenitors generating layer 2/3 PNs and harvested at the following time points: P10 (immature); P15 (branching increasing); P21 (peak of branching); and P35 (adult pattern). Both *Wnk1* and *Wnk2* shRNA knockdowns significantly reduce terminal branching of the callosal axons that reached the contralateral side and also reduce the total number of axons present at P35 (see also Figure S9 for images of axons present at the midline at these time points). The numbers in the bottom left corner of each image correspond to the number of electroporated neurons on the ipsilateral side of each corresponding section. These neuron counts were performed using a machine-learning-based segmentation tool (Ilastik—see STAR Methods for details) and used to normalize the optical density measurements of tdTomato+ axons.

(legend continued on next page)

morphogenesis starting at the early sprouting stage, where a strong reduction in filopodial extensions is already visible at 30 h of pupal development. Throughout the entire axon branching period, we detected a reduction of the overall number of filopodia (Figure 3T). At subsequent stages, axon branches grow and continue to extend but follow erroneous paths and with strong deficits in spatial patterning of axon collaterals (Figures 3J–3M and 3P–3S). We observed these mutant phenotypes with abnormal axon growth and branch patterning using knockdown or MARCM analysis of null mutant neurons. These results exclude the possibility that mechanosensory axons might first develop normally but then regress by limited degeneration of terminal axon branches. In contrast, they support a requirement of dWnk in filopodial and axon branch extension and stabilization as well as axon branch guidance.

Wnk function in axonal morphogenesis is conserved in mouse cortical PNs

dWnk has four related orthologs in mammals named WNK1–4, and several studies have shown that, in particular, WNK1 and WNK4 have prominent roles in the regulation of ion homeostasis in mammalian kidneys (Richardson et al., 2008; Shekarabi et al., 2008, 2017). Given the striking neurodevelopmental defects due to loss of dWnk in mutant *Drosophila* neurons, we investigated whether mammalian WNK kinases play evolutionary conserved roles in axon branching and axon maintenance using mouse cortical PNs, which are long-range projecting principal glutamatergic neurons in the mammalian cortex.

Using a public database (Genepaint) for mRNA expression by *in situ* hybridization (ISH) in mouse embryo at embryonic day (E) 14.5, *Wnk1* mRNA displays a ubiquitous expression and is expressed strongly in the periventricular region of the developing brain, including the cortex (arrow in Figure S5A). *Wnk2* mRNA expression is largely restricted to the CNS with high expression in the developing cortex (arrow in Figure S5B). *Wnk3* and *Wnk4* were not detected by ISH in the developing CNS at E14.5 (Figures S5C and S5D). Interestingly, the same general trend was found in adult mouse brain using a different database (Allen Brain Institute), where ISH revealed that *Wnk1* and *Wnk2* are expressed broadly in all regions of the CNS, but *Wnk3-4* mRNA are not detectable (Figures S5E–S5H). Finally, to determine whether the same trend of adult expression found in mouse brain applied to various cell types in the adult human cortex, we used a publicly available single-cell RNA sequencing (scRNA-seq) database (UCSC Cell Browser). This revealed the same trend as in adult mouse brain, showing that, in the human cortex, *WNK1* and *WNK2* share a highly similar cell type expression pattern being most abundant in principal PNs from layer 2/3, 4, and 5/6 as well as in cortical interneuron sub-populations and some non-neuronal cell types (Figures S6A and S6B), whereas *WNK3* and *WNK4* are almost completely absent from any adult human cortical cell types (Figures S6C and S6D).

To investigate whether the mouse *Wnk1* and/or *Wnk2* are required for axon growth and branching of cortical PNs, we performed *in utero* cortical electroporation (IUCE) of short hairpin RNA (shRNA) encoding plasmids targeting *Wnk1* or *Wnk2* (Figure S7) at E15.5, in order to target cortico-cortical projecting layer 2/3 PNs in the primary somatosensory cortex. Brains of electroporated mice were harvested at various postnatal stages: (1) at postnatal day (P)10, an immature stage when axons have reached the contralateral hemisphere but just started to defasciculate and invade the cortex, where they are still undergoing terminal branching (Figure 4A); (2) at P15, an intermediate stage where axons are progressively increasing their branching in their target layers 2/3 and 5 (Figure 4B); (3) at P21, a juvenile stage with adult-like terminal branching of callosal axons (Figure 4C); and (4) at P35, an adult stage. In layer 2/3 PNs expressing either *Wnk1* shRNA (Figures 4E–4H) or *Wnk2* shRNA (Figures 4I–4L), a population of axons reach the contralateral hemisphere at P10 (Figures 4E and 4I), but terminal axon branching is severely affected through the intermediate stages (Figures 4F, 4G, 4J, and 4K), never reaching wild-type control levels even at adult stages with only a few axons left at P35 (Figures 4H and 4L). Quantification of the optical density from tdTomato+ axons throughout all cortical layers normalized by the total number of electroporated cell body of layer 2/3 PNs on the ipsilateral side demonstrates that *Wnk1* or *Wnk2* shRNA-expressing axons are severely reduced on the contralateral side compared to control shRNA-expressing axons at all stages examined (Figures 4M–4P).

Analysis of axon density at the midline (corpus callosum) in *Wnk1* or *Wnk2* shRNA-expressing neurons confirm that axons successfully cross the midline and are present from P10 to P21 but show significant reduction in number by P35 compared to control (Figures S8A–S8L).

To quantify axon growth and branching at single-cell resolution, we turned to *ex utero* cortical electroporation (EUCE) followed by dissociated culture *in vitro* as previously described (Courchet et al., 2013). We compared axon morphology in control, WNK1 overexpression (OE), as well as *Wnk1* or *Wnk2* shRNA-mediated knockdown conditions. Compared to control neurons, overexpression of WNK1 led to longer axons, with more collateral branches (Figures S9A and S9B). Conversely, shRNA-mediated knockdown of either *Wnk1* or *Wnk2* resulted in cortical PNs with shorter and less-branched axons (Figures S9C and S9D). Quantifications confirmed a dose-dependent effect of WNK1 on axon length and collateral branching (Figures S9E–S9G). *Wnk1* or *Wnk2* knockdown led to a similar reduction of axon length and collateral branching without any additive effect of the double knockdown of *Wnk1* and *Wnk2* (Figures S9H–S9J), suggesting they belong to the same pathway. Interestingly, effect of *Wnk1* knockdown or overexpression is restricted to axon morphogenesis because we did not observe any consequence of *Wnk1* modulation (WNK1 overexpression

(M–P) Optical density measurements of tdTomato+ axons on the contralateral side normalized by the number of electroporated neurons on the ipsilateral side of each section. Three sections from each brain were quantified. $n_{pLKO\ P10} = 3$; $n_{pLKO\ P15} = 3$; $n_{pLKO\ P21} = 5$; $n_{pLKO\ P35} = 5$; $n_{WNK1\ P10} = 4$; $n_{WNK1\ P15} = 3$; $n_{WNK1\ P21} = 3$; $n_{WNK1\ P35} = 5$; $n_{WNK2\ P10} = 3$; $n_{WNK2\ P15} = 3$; $n_{WNK2\ P21} = 4$; $n_{WNK2\ P35} = 3$. Statistical analysis: a two-way ANOVA followed by multiple Tukey's comparisons test: *$p < 0.05$; **$p < 0.01$; ***$p < 0.001$; ****$p < 0.0001$.
Scale bar in (A)–(L): 100 μm.

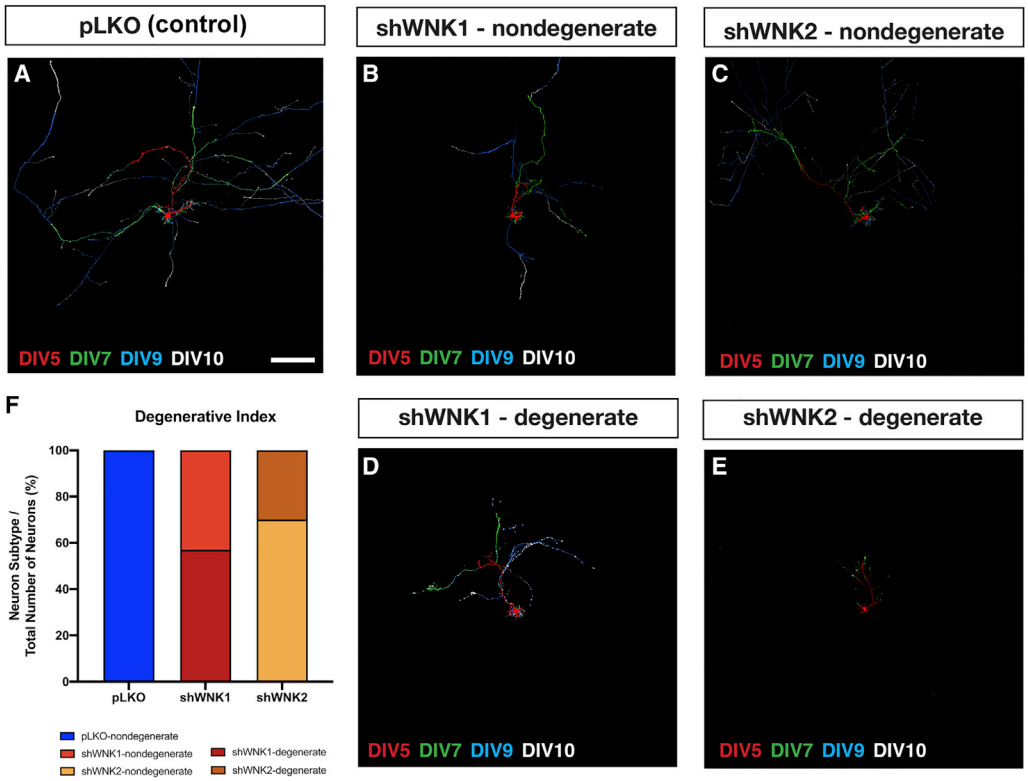

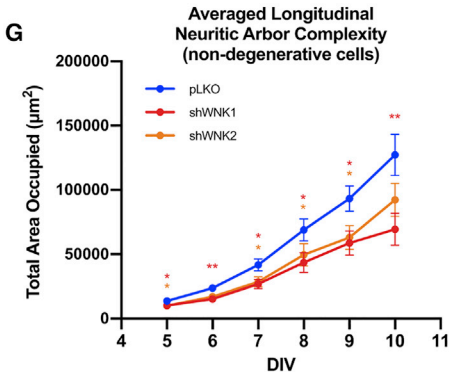

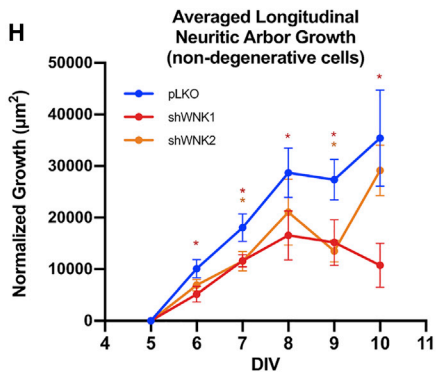

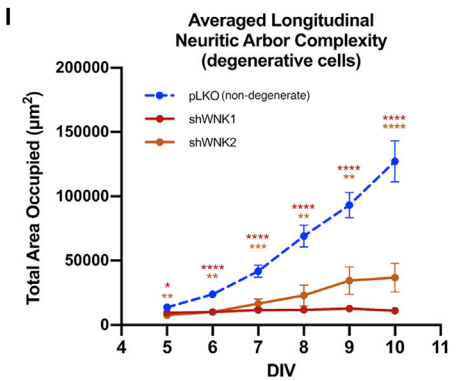

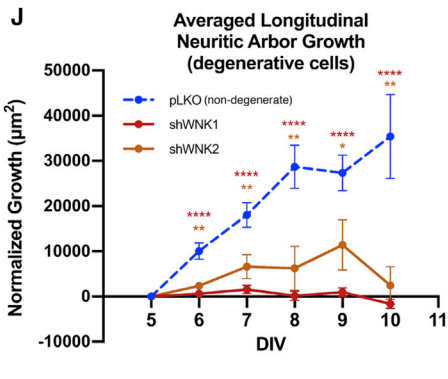

(legend on next page)

or *Wnk1* knockdown) on dendritic morphology at 21 days *in vitro* (DIV) (Figures S9K–S9M). This is consistent with results presented above (Figures S3I–S3L) showing that loss of dWnk in *Drosophila* DCN and sensory ddaE-class I neurons leads to strong axonal but no dendritic morphogenesis defects within the same neurons.

To further confirm that WNK1 and WNK2 affect axon growth and branching, we performed time-lapse imaging of axonal development over 16 h (10-min imaging interval) and quantified axon elongation and branch formation (Figures S10A and S10B). Axon elongation was disrupted by a failure to consolidate growth at the tip of the axon. Indeed, short periods of growth cone progression (Figure S10C, green arrowhead) alternated with growth cone retraction (purple arrowhead) and initiation of an alternative growth cone from an above position on the axon shaft. Although the growth cone speed during the periods of growth was identical in control and knockdown condition, we measured a reduced time spent growing and increased pause duration in *Wnk1* and *Wnk2* knockdown neurons, resulting in a net decrease of axon elongation (Figures S10D–S10G). Finally, we measured that branch dynamics were altered with a decrease of the fraction of new, stable branches created and an increase in transient (<2 h) branches (Figure S10H). Altogether, these results demonstrate that mouse WNK1 and WNK2 are directly involved in axon development similarly to their *Drosophila* counterpart.

Wnk1 and Wnk2 are required in axon maintenance in developing neurons

Following expression of Wnk1 or Wnk2 shRNA, we observed a gradual, significant reduction in mVenus+ axonal labeling in the corpus callosum at the midline compared to control shRNA (Figures S8A–S8L) and a marked loss of axon branching both *in vivo* (Figure 4) and *in vitro* at least at early stages of neuronal differentiation (Figure S9). These data suggest that *Wnk1* or *Wnk2* are not only required for axon branching but might also be required for axon maintenance.

We used very sparse EUCE in order to obtain individual cortical PNs that can be optically isolated and performed time-lapse analysis by repetitively imaging individual neurons once every 24 h from 5 to 10 DIV (Figure 5A). In cortical PNs expressing control shRNA, we observed progressive but extensive axon growth and branching (Figures 5A, 5F, and 5G; see Videos S1 and S2) but never spontaneous axon fragmentation and degeneration in these culture conditions.

Cortical PNs expressing *Wnk1* or *Wnk2* shRNA display two classes of phenotypes: in ~55% cortical PNs expressing *Wnk1* shRNA (Figure 5B) and ~65% of cortical PNs expressing *Wnk2* shRNA (Figure 5C), we observed reduced axon growth and branching but no sign of axon fragmentation or degeneration at least by 10 DIV (Figure 5F; see also Videos S3 and S5). Furthermore, in the remaining ~45% of cortical PNs expressing *Wnk1* shRNA and ~35% of cortical PNs expressing *Wnk2* shRNA, we observed initially reduced axon growth and branching followed by striking patterns of rapid axon fragmentation and degeneration occurring between 7 and 8 DIV (Figures 5D–5F; Videos S4 and S6). Quantification of the dynamics of axon growth and branching (cumulative axon length and area; Figures 5G and 5I) or normalized growth rate (increase in total axonal length per day; Figures 5H and 5J) demonstrated that axon growth and branching is significantly reduced in axons expressing *Wnk1* or *Wnk2* shRNA in both classes of axons.

Our *ex utero* electroporation protocol is performed in both cases at E15, targeting the progenitors lining the ventricular zone at that time, which generate exclusively layer 2/3 PNs in the dorsal telencephalon. However, the limitation of this approach is that, upon electroporation, the neural progenitors pick up various amount of the plasmid and subsequently can divide several times to generate layer 2/3 PNs, thereby creating a "mosaic" expression of cDNA- or shRNA-encoding plasmids. We favor this explanation to describe the range of phenotypes obtained, leading to two extreme phenotypes upon Wnk1 or Wnk2 shRNA-mediated knockdown: (1) one class of neurons where axon branching and growth is affected, but not axon maintenance (presumably the neurons where knockdown of Wnk1 or 2 is suboptimal) and (2) a second class of neurons where axon branching and maintenance is affected (presumably the neurons where knockdown of Wnk1 or 2 is above a certain threshold). This interpretation is reinforced by the analysis performed in *Drosophila*, where neurons expressing 1× RNAi (expressed genomically here) show severe axon branching defect, but not axon degeneration, and neurons expressing 2× RNAi show initially axon branching defects but ultimately axon degeneration (Figure 2).

Wnk1 and Wnk2 are required for axon maintenance in adult neurons

In order to directly test whether Wnk1 and Wnk2 are required for axon maintenance in adult mouse cortical PNs, we developed a new experimental approach that enables inducible expression of

Figure 5. *Wnk1* and *Wnk2* control axon branching and degeneration in cortical pyramidal neurons *in vitro*

(A–E) Representative cortical layer 2/3 pyramidal neurons imaged longitudinally at 5, 6, 7, 8, 9, and 10 DIV with only 5, 7, 9, and 10 DIV *ex utero* electroporated with control shRNA (pLKO-scramble; A) or with shRNA targeting *Wnk1* (B and D) or *Wnk2* (C and E). We distinguished two classes of neurons based on their phenotypes: neurons that showed clear signs of degeneration (axon blebbing and ultimately cell fragmentation; B and C) and neurons that did not show any sign of degeneration at least during the 10 DIV (D and E). Neuronal morphology was visualized by tdTomato expression and pseudo-colored to represent consecutive days of imaging.

(F) Quantification of ultimate neuronal fate at 10 DIV for the pLKO, shWNK1, and shWNK2 conditions as determined by the presence (degenerate) or absence (non-degenerate) of neuronal fragmentation.

(G–J) Quantification of axonal arbor complexity and growth as measured by the total area occupied by the axon (G and I) of either non-degenerate (G) or degenerate (I) neurons and by the axon growth rate (H and J) as measured by the total area occupied by the axon cumulatively gained each day for both non-degenerate (H) and degenerate (J) neurons. Statistical analyses: non-parametric Mann-Whitney test comparing each condition at each time point, with the data presented in (G)–(J) as mean and SEM. Number of neurons for quantification: $n_{pLKO} = 19$; $n_{shWNK1} = 28$; $n_{shWNK2} = 23$ from at least three independent experiments. Significance: *$p < 0.05$ with the following criteria: *$p < 0.05$; **$p < 0.01$; ***$p < 0.001$; and ****$p < 0.0001$.

Scale bar in (A)–(E): 100 μm.

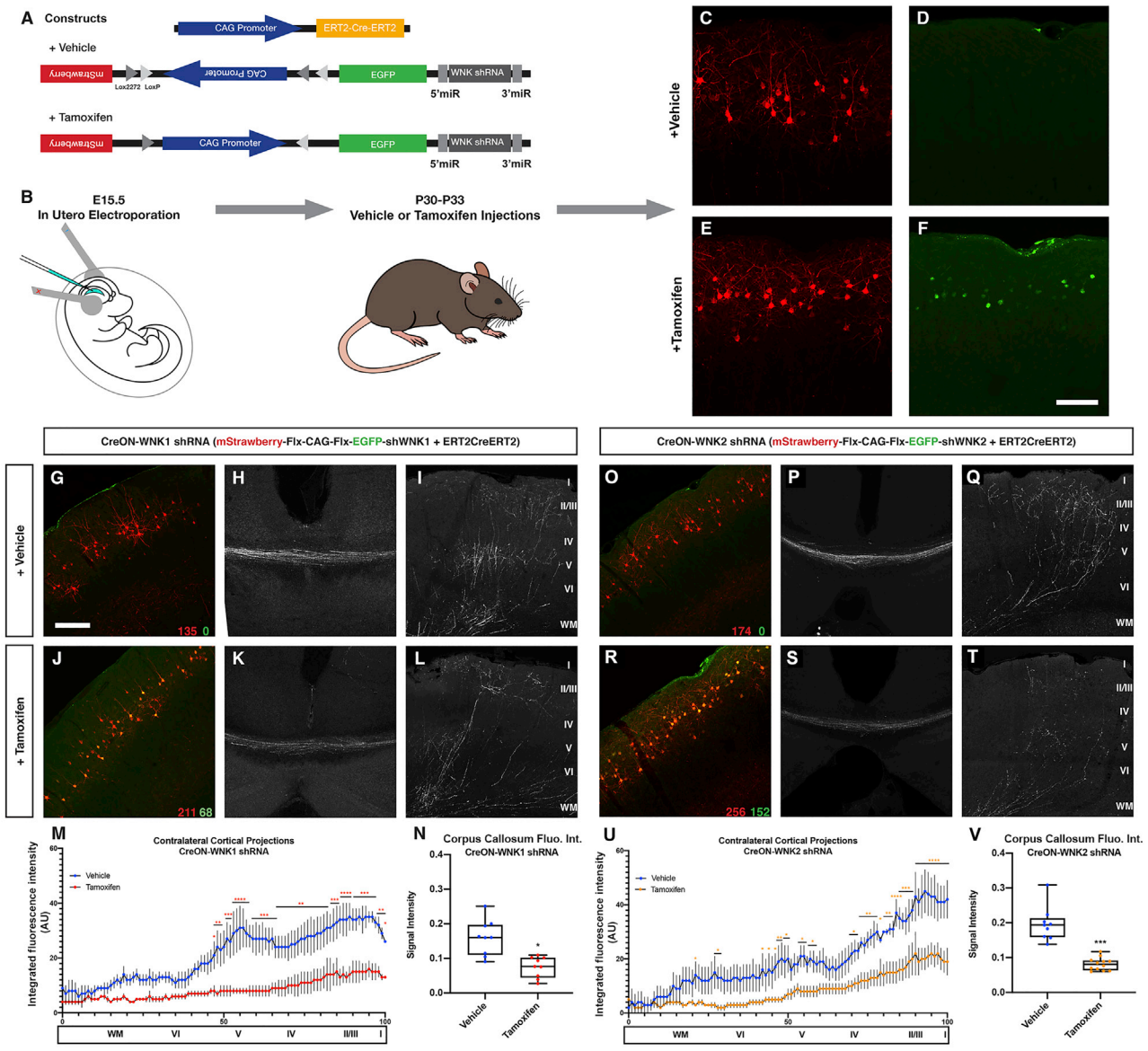

Figure 6. Adult knockdown of *Wnk1* or *Wnk2* causes axonal degeneration in mouse cortical layer 2/3 pyramidal neurons

(A and B) Design of the conditional shRNA expression plasmids (CreON-shWNK) used to achieve inducible, adult knockdown of *wnk1* and *wnk2* in layer 2/3 PNs of the mouse cortex. Our strategy uses co-electroporation of a tamoxifen-inducible form of Cre recombinase (ERT2-Cre-ERT2) in combination with a plasmid where a cytomegalovirus (CMV) enhancer/chicken-β-Actin promoter (CAG) cassette flanked by incompatible Lox sites (Lox2272 and LoxP; subsequently referred to as FLEX plasmid) drives the expression of a fluorescent mStrawberry protein in absence of tamoxifen. In the presence of tamoxifen, Cre recombines the CAG promoter and flips its orientation to drive the expression of a mRNA coding for EGFP and WNK shRNA (after 5′ and 3′ microRNA [miRNA] processing). Our experimental design (B) is as follows: at E15.5, mice undergo *in utero* electroporation with the CreON-shWNK plasmid and tamoxifen-dependent pCA-G::ERT2-Cre-ERT2; at P30–P33, adult mice undergo four (one per day) consecutive intraperitoneal injections with tamoxifen diluted in corn oil (0.1 mg/g of bodyweight) or control vehicle only (corn oil); and at P37 (8 days following first injection), mice were perfused and their brains sectioned, immuno-amplified, and imaged.

(C–F) Representative images of adult layer 2/3 PNs on ipsilateral side relative to *in utero* electroporated cortex of mice injected with vehicle (C and D) or with tamoxifen (E and F).

(G–L) Detail of a coronal brain section of a P37 mouse *in utero* co-electroporated with CreON-shWNK1 and ERT2CreERT2 showing (H and K) a reduction of callosal axonal projections and (I and L) a reduction in contralateral axonal branching upon adult knockdown of WNK1. Red inset numbers indicated the number of electroporated PNs; green inset numbers represent the number of EGFP+ PNs.

(legend continued on next page)

shRNA *in vivo*. Our strategy revolves around two parts (Figures 6A and 6B): (1) we used IUCE (E15) to co-express a plasmid expressing a tamoxifen-inducible form of Cre (ERT2-Cre-ERT2) and a novel plasmid expressing the red fluorophore mStrawberry in the absence of tamoxifen but upon tamoxifen-dependent Cre activation; the CAG promoter and enhancer cassette orientation is flipped, leading to expression of a bi-cistronic mRNA encoding EGFP and a Wnk1 or Wnk2 shRNA upon mRNA processing (Figure 6A). We performed tamoxifen induction of Cre-mediated recombination (and induced shRNA expression) using four daily tamoxifen intraperitoneal (i.p.) injections at P30–P33. This approach is robust because, in the absence of tamoxifen, we observed many mStrawberry-expressing layer 2/3 PNs (Figure 6C), but we never EGFP co-expressing neurons (Figure 6D; see also Figures 6G and 6P). However, in mice injected with tamoxifen, we observed a large fraction of layer 2/3 PNs co-expressing EGFP at various levels (~30%–50% co-expression; Figures 6E and 6F).

This approach therefore allowed us to test whether inducible shRNA knockdown of Wnk1 or Wnk2 in adult layer 2/3 PNs is required for axon maintenance. 7 days following the first tamoxifen injection (i.e., at P37) or injection of vehicle (corn oil) for the control group, we imaged axons of layer 2/3 PNs at the midline (corpus callosum) or on the contralateral side, where they undergo terminal axon branching. Both Wnk1 and Wnk2 shRNA expression leads to significant reduction of the fraction of axons relative to the number of electroporated neurons at the corpus callosum (Figures 6K and 6T) and on the contralateral side (Figures 6L and 6U) compared to control (Figures 6H, 6I, 6Q, and 6R). Quantification of optical density of mStrawberry+ axons on the contralateral side (normalized to number of electroporated neurons) demonstrates a significant reduction in axon density in Wnk1 shRNA-expressing neurons (Figure 6M) or Wnk2 shRNA-expressing neurons (Figure 6V) compared to control. The same significant reduction in optical density of mStrawberry+ axons at the midline is observed in Wnk1 or Wnk2 shRNA-expressing axons compared to control (Figures 6N and 6W). These results demonstrate that Wnk1 and Wnk2 are required for axon maintenance in adult mouse PNs.

Loss of Nmnat and gain of dSarm or Axed disrupts axon branching during development

Mammalian WNK1 and WNK4 are known to regulate two downstream kinases (i.e. serine-threoninie kinase OSR1 and STE20/SPS1-related proline/alanine-rich kinase) (OSR1/SPAK) and target the sodium Na^+:Cl^- cotransporter (NCC)/potassium KCL (KCC) cotransporters in kidney cells (Vitari et al., 2005; Moriguchi et al., 2005; Anselmo et al., 2006; Gagnon et al., 2006). This regulation is essential for blood pressure regulation (Richardson and Alessi, 2008; Wu et al., 2019; Hadchouel et al., 2016). Disruption of these WNK-dependent functions constitutes the basis of hypertension in several hereditary human diseases (Rafiqi et al., 2010). In order to explore the molecular mechanisms underlying WNK function in axon branching and degeneration, we initially tested whether downregulation of Frayed, the *Drosophila* ortholog of OSR1 and SPAK kinases, or NCC and KCC phenocopied dWnk LOF axon branching defects. However, we could not detect dWnk-like axonal branching defects upon RNAi knockdown of Frayed or KCC (Figure S11).

In our efforts to identify other potential factors mediating the function of dWnk, we tested previously identified effectors of axon maintenance (Gilley and Coleman, 2010; Neukomm et al., 2017; Babetto et al., 2013; Conforti et al., 2014; Essuman et al., 2017). In a candidate screen, we discovered that LOF and RNAi knockdown of Nmnat in mechanosensory neurons leads to axon branching defects remarkably similar to dWnk LOF defects (Figures 7A and 7C–7E). A previous study provided evidence that reduction of Nmnat in *Drosophila* sensory neurons leads to activation of dSarm as well as a newly identified protein Axundead (Axed) to execute axon degeneration (Neukomm et al., 2017). Consistent with these findings, we found that overexpression of Axed or dSarm caused axon branching defects similar to loss of dWnk or loss of Nmnat (Figures 7F and 7G). These results provide evidence that Nmnat is required developmentally for axon branching of mechanosensory neurons. Moreover, overexpression of Axed or dSarm during axon development resulted in axon branching defects remarkably similar to loss of dWnk or Nmnat.

dWnk regulates axon branching and maintenance by regulating Nmnat, dSarm, and Axed

In order to address the functional relationship of dWnk and these components, we used genetic epistasis analysis (Figures 7 and S12). We found that both loss of Axed and dSarm can suppress the axon branching defects in dWnk mutant neurons (Figures 7C, 7I, 7J, 7O, S12A–S12E, and S12Q) and prevents loss of axons (Figures 7S, 7T, 7W, 7X, S12K–S12M, and S12R). Conversely, the gain of function branching defects and loss of axons upon Axed and dSarm overexpression can be suppressed

(M and N) Quantification of RFP fluorescence (±SEM) in mice *in utero* electroporated with CreON-shWNK1 and ERT2CreERT2 along the radial axis of the cortical wall in the contralateral cortex (M) or corpus callosum (N) at P37 in mice previously injected with either vehicle or tamoxifen, normalized to the total number of electroporated cells.

(O–T) Representative coronal brain section of a P37 mouse *in utero* electroporated with CreON-shWNK2 and ERT2CreERT2, showing tamoxifen induction of EGFP-miRNA expression in (R) (but not in control—O), a reduction of callosal axonal projections (compare P and S) and a reduction in contralateral axonal branching upon adult knockdown of WNK2 (T) compared to control (Q). Red inset numbers indicated the number of electroporated PNs; green inset numbers represent the number of EGFP+ PNs.

(U and V) Quantification of RFP fluorescence (±SEM) in mice *in utero* electroporated with CreON-shWNK2 and ERT2CreERT2 along the radial axis of the cortical wall in the contralateral cortex (U) or corpus callosum (V) at P37 in mice previously injected with either vehicle or tamoxifen, normalized to the total number of electroporated neurons.

Statistical analyses: Mann-Whitney test (N) and (W) or a two-way ANOVA followed by Tukey's multiple comparisons test (M) and (V): $^*p < 0.05$; $^{**}p < 0.01$; $^{***}p < 0.001$; $^{****}p < 0.0001$. Number of mice for each experimental condition: $n_{CreON\text{-}shWNK1\ +\ vehicle} = 3$; $n_{CreON\text{-}shWNK1\ +\ tamoxifen} = 3$; $n_{CreON\text{-}shWNK2\ +\ vehicle} = 3$; $n_{CreON\text{-}shWNK2\ +\ tamoxifen} = 4$. At least 3 sections analyzed per brain as described for Figure 4 are shown.

Scale bars in (C)–(F): 150 μm; (G)–(U): 100 μm.

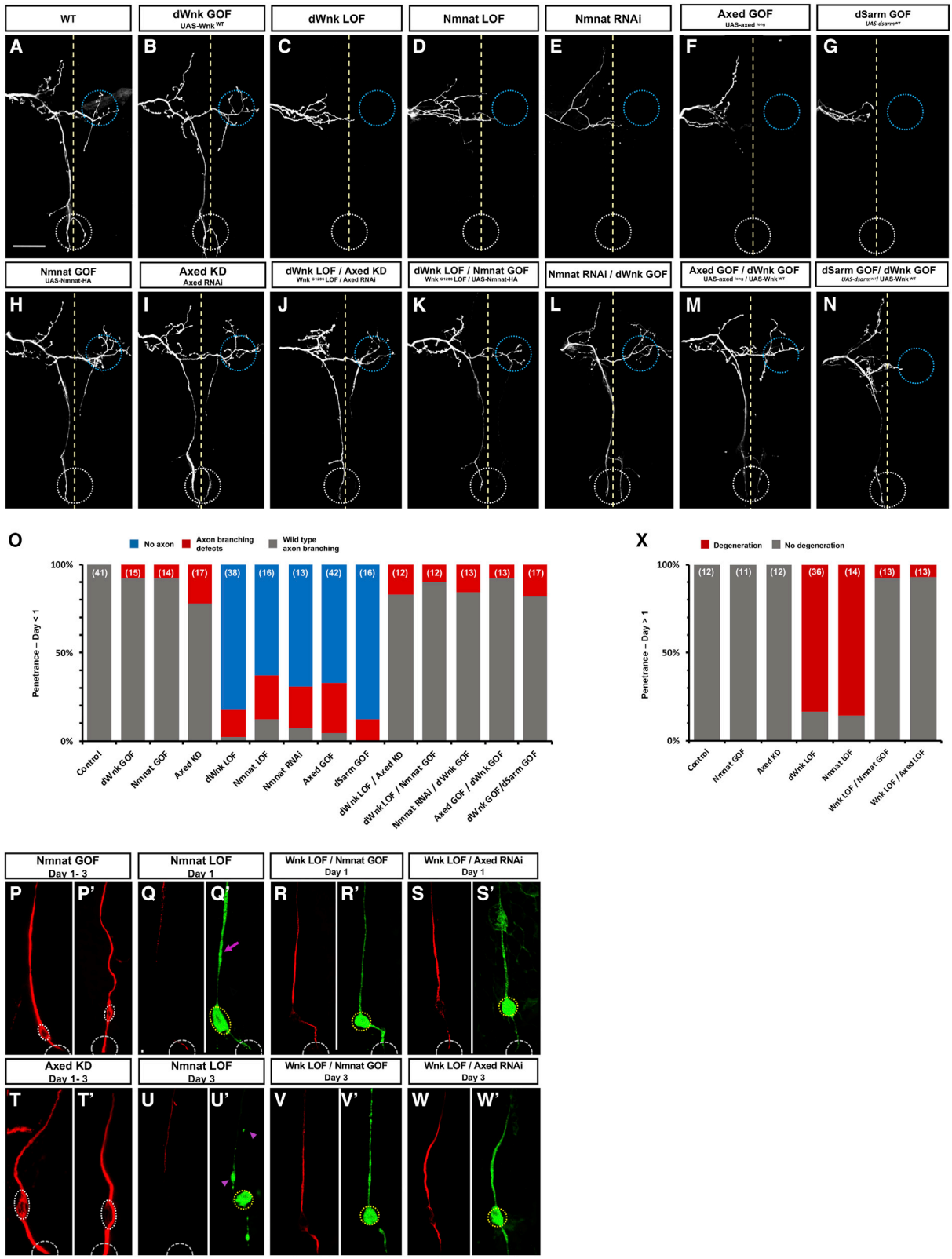

(legend on next page)

by co-overexpression of dWnk (Figures 7F, 7G, 7M–7O, S12F–S12J, S12N–S12P, and S12R). This argues for an antagonistic functional relation between dWnk and the axon destruction factors Axed and dSarm during axon branching as well as maintenance.

Overexpression of dWnk or Nmnat alone did not result in any dominant phenotypic defects (Figures 7B and 7H). However, we found that the axon branching defects characteristic for dWnk mutant neurons can be suppressed by Nmnat overexpression (Figures 7C, 7H, 7K, and 7O). Conversely, axon branching defects characterizing Nmnat RNAi knockdown neurons can be rescued by overexpression of dWnk (Figures 7E, 7L, and 7O). We further observed that overexpression of Nmnat in pSc neurons can also suppress or slow down the degeneration of axons in dWnk mutant neurons (Figures 7P–7R, 7U, 7V, and 7X). In summary, the genetic analysis of fly mechanosensory neurons suggest that dWnk functions synergistically with Nmnat in order to prevent gain of activity of dSarm and Axed, which can disrupt both (1) axon branching during development and (2) axon maintenance in mature neurons.

Wnk and Nmnat proteins can form complexes and are depleted by Sarm1 activity

We conducted a series of biochemical immunoprecipitations to test potential protein interactions of dWnk as well as mammalian WNK1/2 with the axon maintenance or destruction factors examined in the genetic analysis (Figure 8). We found that immunoprecipitation of endogenous dWnk from S2 cell extracts can pull down tagged dNmnat (Figure 8A). This is consistent with published findings, where dWnk was identified by mass spectrometry from a complex co-purified with Nmnat overexpressed in fly brains (Ali et al., 2016). For the mammalian homologs Wnk1/2, we found that Nmnat2 can be co-immunoprecipitated with Wnk1, suggesting conserved Wnk-Nmnat interactions. We found that these interactions are likely occurring via the N-terminal part of Wnk1 and to a lesser degree with the kinase domain of Wnk1 itself (Figure 8B). We further found that Wnk1 can be immunoprecipitated with Wnk2 and vice versa (Figure 8C), consistent with the finding that both kinases are functionally required in mouse PNs.

We further tested potential dWnk interactions with the axon destructive factors Axed and dSarm. We found that co-expressed Axed (V5-tagged) and dWnk could form complexes in *Drosophila* S2 cells (Figure S13A). *Drosophila* Axed is a member of the large Broad-Complex, Tramtrack and Bric a brac (BTB-domain)-containing family of proteins. Although currently no functional mammalian ortholog of Axed is known, we found that mammalian Wnk2 has the potential to interact with *Drosophila* Axed and a subset of related BTB-domain-containing proteins (Figures S13B–S13F). In contrast, the functional conservation of *Drosophila* dSarm and mammalian Sarm1 is well documented by molecular and genetic studies. We therefore tested the potential molecular interactions of the axon-protective WNK1 and WNK2 kinases and degeneration effector SARM1. Surprisingly, however, co-overexpression of SARM1 with either WNK1 or WNK2 caused a strong decrease in both WNK1 or WNK2 protein abundance (Figures 8D and 8G). Yet by testing different expression levels of SARM1 and WNK1 or WNK2, we nevertheless were able to co-immunoprecipitate SARM1 and WNK1 or WNK2 (Figures S14A and S14B). Importantly, the co-expression experiments revealed not only that SARM1 protein overexpression either directly or indirectly triggers rapid depletion of WNK1 and WNK2 in HEK293T (Figure 8D; quantification in Figure 8G) or SH-SY5Y cells (Figure S14B) but also that NMNAT1 as well as NMNAT2 levels were nearly completely depleted when co-expressed with SARM1 (Figures 8E and 8F; quantification in Figure 8G). Application of commonly used inhibitors of proteasomal degradation to cells co-expressing Sarm1 and Wnk2 or Nmnat2 did not block this depletion of Wnk2 and Nmnat2 protein (Figure S14B). We further detected no decrease in mRNA expression of Wnk1/2 or Nmnat1/2 upon overexpression of Sarm1 (Figure S14C). It has been reported that Nmnat2 protein is labile and has a rapid turnover time, whereas the mutant (and axon-protective) Nmnat-fusion protein Wallerian degeneration slow (WldS) is significantly more stable (Coleman and Freeman, 2010). Consistent with previous reports and this hypothesis, we found that blocking *de novo* protein synthesis in cells expressing Nmnat2 by addition of cycloheximide, Nmnat2 protein, but not WldS, is rapidly lost (Figure S14E).

Figure 7. Genetic epistatic analysis reveals that dWnk positively enhances Nmnat function and negatively regulates Axed and dSarm in the control of both axon branching and axon maintenance

(A–N) Representative confocal images of mechanosensory neurons dye filled with carbocyanine dyes.

(A) WT mechanosensory neurons displaying the stereotyped branching pattern.

(C–G) dWnk loss of function (LOF), Nmnat LOF, Nmnat RNAi, Axed overexpression (gain of function, GOF), and overexpression of dSarm are showing very similar phenotype, i.e., axon branching defects with loss of distal axon terminals.

(B, H, and I) overexpression of dWnk and Nmnat as well as Axed knockdown are showing normal branching pattern.

(J and K) dWnk LOF-induced axon branching defects can be rescued by Axed RNAi knockdown and overexpression of Nmnat, which is showing normal branching pattern.

(L–N) Overexpression of dWnk can maintain the axonal branches otherwise disrupted by Nmnat RNAi, Axed GOF, and dSarm GOF.

(O) Quantification of axonal branching defects observed in the various conditions described above.

(P–W) Visualizing distal to proximal axon degeneration of mechanosensory neurons in thorax at day 1 and 3.

(P and T) Nmnat OE and Axed knockdown are showing a near continuous labeling of the microtubule cytoskeleton using anti-22C10 antibody staining same as WT control samples.

(Q and U) Genetic mosaic analysis of Nmnat homozygous mutant mechanosensory neurons shows that lacking Nmnat leads to axon swelling and blebbing (arrows in magenta) in 1-day-old samples followed by axon fragmentation and clearance of axonal debris (arrowheads in magenta) in 3-day-old samples.

(R and V) Overexpression of Nmnat can rescue the axon degeneration caused by loss of dWnk.

(S and W) Knockdown of Axed prevents axon degeneration caused by dWnk LOF.

(X) Quantification of axon degeneration in mechanosensory neuron proximal to the cell body located in thorax in the various conditions described for (P)–(W'). Scale bar: 20 μm.

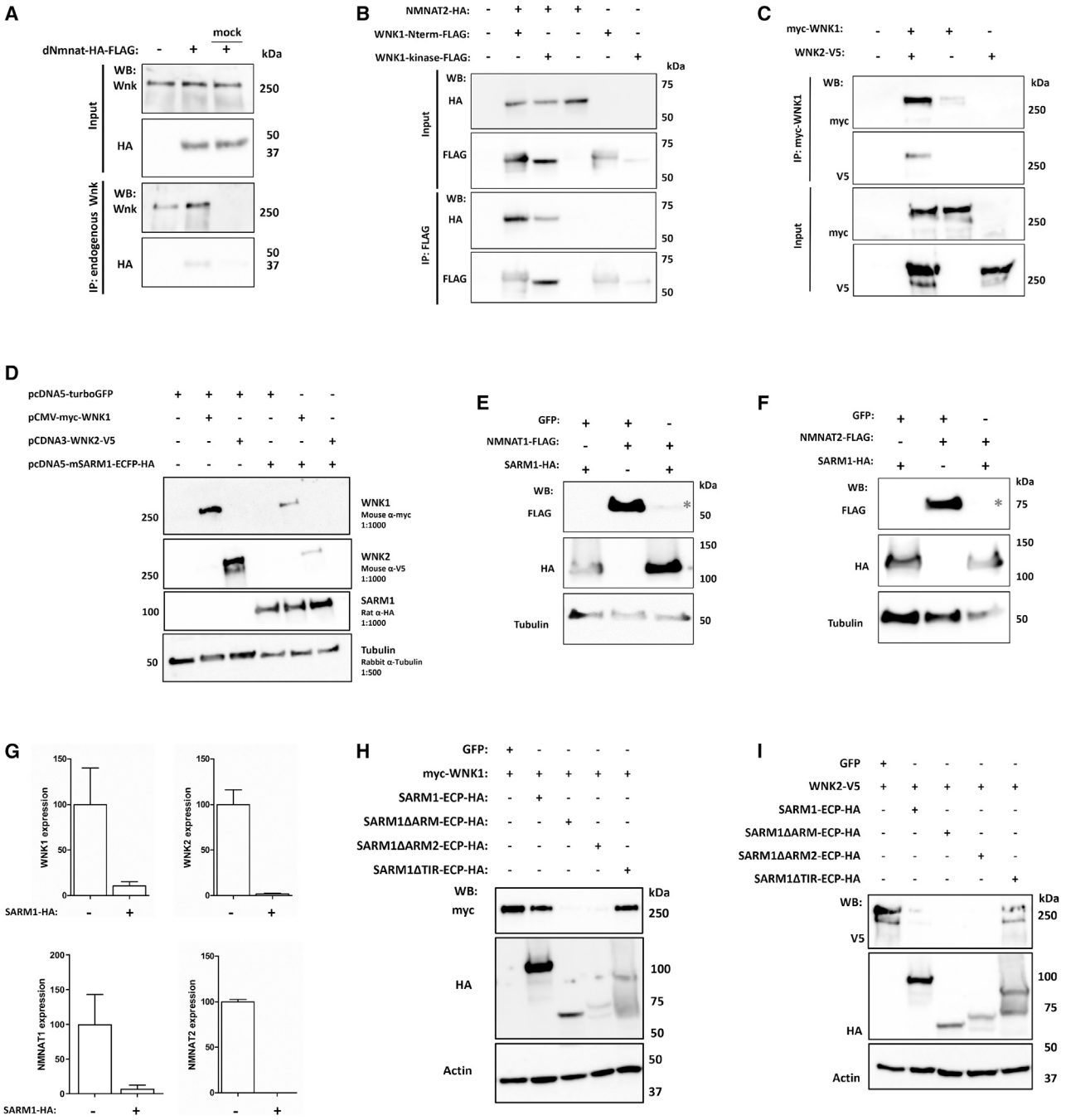

Figure 8. SARM1-dependent downregulation of Wnk and Nmnat

(A) dWnk interacts with dNmnat. dNmnat expression was induced using $CuSO_4$ in stable *Drosophila* S2 cells. Endogenous dWnk was precipitated using magnetic beads, and co-precipitated protein complexes were analyzed using an hemagglutinin (HA)-tag-specific antibody. Non-coated beads were used as mock control.

(B) The mammalian N-terminal domain of WNK1 interacts more stringently with mammalian NMNAT2 than its kinase domain. Validation of interactions by co-immunoprecipitation is shown. HEK293T cells were co-transfected with rat WNK1 domains together with human HA-tagged NMNAT2. WNK1 domains were precipitated using anti-FLAG magnetic agarose. Co-precipitated protein complexes were analyzed by western blot (WB) using an HA-tag-specific antibody.

(C) Mammalian WNK1 and WNK2 are interacting. Validation of interaction by co-immunoprecipitation is shown. SH-SY5Y cells were co- transfected with mammalian myc-tagged WNK1 and V5-tagged WNK2. WNK1 was precipitated using anti-myc magnetic beads, and co-precipitated protein complexes were visualized by WB using a V5-tag specific antibody.

(D–G) SARM1 NAD+ catalytic activity is required for regulation of WNK1, WNK2, and NMNAT2 expression. WB images and quantification of expression of myc-tagged WNK1 and WNK2-V5 (D), NMNAT1-FLAG (E), and NMNAT2-FLAG (F) when co-transfected with either a GFP-containing plasmid or SARM1-HA are

(legend continued on next page)

Importantly, Nmnat2 depletion is also more sensitive to Sarm1 overexpression than WldS. We therefore hypothesize that one potential mechanism by which Sarm1 could trigger depletion of Wnk or Nmnat proteins is through inhibition of *de novo* protein synthesis. The direct target of Sarm1 underlying this translational control is currently not known. However, testing different mutant forms of Sarm1 provided evidence that this potential translational control function of Sarm1 requires its catalytic nicotinamide adenine dinucleotide (NAD+) consuming function (Figures 8H and 8I). Specifically, we co-expressed Wnk1 (Figure 8H) and Wnk2 (Figure 8I) with Sarm1 protein forms that enhance or lack catalytic activity. We found that dominant active Sarm1 mutants are even more potent than wild-type Sarm1 in depleting Wnk1 and Wnk2 protein. In contrast, a Sarm1 mutant that lacks the catalytic domain is not able to deplete Wnk1 or Wnk2 protein (Figures 8H and 8I). Although it is known that Nmnat can enzymatically increase NAD+ levels, it is unclear how Wnk proteins exert their role in axon protection. We found, however, that dWnk wild-type function as well as its ability to suppress dSarm gain of function depend on its kinase activity (Figure S15).

Together, these results suggest that the degeneration effector SARM1 is capable of downregulating WNK and NMNAT expression when co-expressed in cell culture. This *in vitro* result is consistent with our genetic epistasis experiments showing antagonistic relations between dWnk/Nmnat and dSarm.

DISCUSSION

In this study, we report that the function of the Wnk-family kinases (*Drosophila* dWnk and mammalian WNK1/2) are required in developmental axonal branch patterning as well as axon maintenance. We show that phenotypic defects observed in mechanosensory axons of dWnk mutant neurons are indistinguishable from defects observed in Nmnat mutant neurons. Both dWnk and Nmnat mutant mechanosensory axons can grow from the periphery to the VNC but require dWnk as well as Nmnat function during axonal branch growth and patterning. Moreover, a post-developmental knockdown of dWnk triggered progressive degeneration in mature and fully developed mechanosensory axons. Such an adult-specific function is also analogous to the well-documented role of Nmnat in axon maintenance (Gilley and Coleman, 2010; Wen et al., 2011; Ali et al., 2013; Sasaki et al., 2016). Although Nmnat has been studied most extensively for its role in axon maintenance in injury models or neurodegenerative disease models, it has been reported previously that LOF mutants are lethal and show axonal defects (Huppke et al., 2019; Lukacs et al., 2019). Furthermore, we show here that the dual developmental and maintenance functions of dWnk are evolutionary conserved, as knockdown of WNK1 and WNK2 results in remarkably similar axon morphogenesis defects and trigger axon degeneration in mouse cortical neurons. We conclude that, in neurons, Wnk kinases exert novel functions that are analogous and synergistic to conserved Nmnat functions. The discovery of Wnk kinases having important neuroprotective roles analogous to Nmnat offers new tools and insights to further dissect the complex regulatory network underlying active axon degeneration.

Formally, the adult maintenance defects that we observed upon Wnk depletion could be a consequence of developmental defects. However, several reasons argue strongly against this possibility: first, the *in vivo* knockdown of WNK1 and WNK2 after P30 in mouse cortical layer 2/3 PNs triggered degeneration of axons of mature neurons. Second, knockdown of dWnk at post-developmental (late pupal) stages does not alter the axonal branching or targeting of mechanosensory neurons but triggered spontaneous degeneration of adult mechanosensory axons after 3 days post-eclosion. Third, a single-copy RNAi knockdown of dWnk resulted in strong axon branching defects. Fourth, in previous studies, we identified and characterized several mutants that lead to severe axon branching defects of mechanosensory axons. For example, in Dscam1-null mutant clones, the axon branching defects are even more severe than in dWnk mutant clones, yet we found no sign of axon degeneration even in 1 week or older flies (see examples in He et al., 2014 and Dascenco et al., 2015). Fifth, even in cases of very short axon branches in dWnk or other mutants with a complete absence of contralateral projecting axon collaterals, the distal part of the mutant axons still reaches the corresponding ipsilateral target area. Given that putative trophic signals would have to support axons on both sides of the VNC, it seems highly unlikely that target-derived trophic signals would only support contralateral projecting axon arbors. In summary, our data provide strong evidence that Wnk kinases have dual roles: first, during developmental axon morphogenesis and, second and independently, during continuous axon maintenance in mature neurons.

A key question raised by these results is: how similar are the molecular processes in developmental axon growth and branching and adult maintenance? A related question has been discussed in a hallmark review (Raff et al., 2002). This perspective article discussed the discovery that neurons can activate a self-destructive program independent of general apoptosis. The authors noted that neurons "apparently have a second, molecularly distinct self-destruct program in their axon." And the authors raise the incisive question: "Do neurons also use this second program to prune their axonal tree during development and to conserve resources in response to chronic insults?"

We assume that "pruning of axonal branches during development" could—as a cellular mechanism—also be involved in axonal branch patterning as analyzed here. Specifically, we view the developmental axon branching of mechanosensory axons as a process where continuous competitive interactions among nascent branches select for stabilization or retraction (timescale minutes or few hours). In contrast, the well-characterized pruning of axons during metamorphosis (e.g., mushroom body remodeling) is initiated when axon branches and connectivity have been already established. This type of pruning (remodeling) requires

shown. Graphs represent optical density measurements for indicated bands showing mean ± SEM of 2–4 independent experiments (G). α-tubulin was used as loading control.

(H and I) SARM1$^{\Delta TIR}$-HA does not reduce expression levels of myc-tagged WNK1 (H) and V5-tagged WNK2 (I) to the same extent as full-length SARM1-HA and SARM$^{\Delta ARM}$ mutants. For both WBs, actin was used as a loading control.

primarily a destabilization of a fully established axon projection and is likely different from axonal branch selection as investigated here. Consistent with this idea is the finding that Nmnat is not required in axon pruning of mushroom body neurons (Hoopfer et al., 2006).

Our results now provide genetic and molecular data that support the notion that components of a "distinct self-destruct program" are involved in axon branch stabilization and destabilization. We further suggest that molecular control mechanisms of axon branching and axon destruction (or preventing axon destruction, i.e., axon maintenance) are mechanistically related. Specifically, the dynamics of axon branching requires the selection of an exuberant number of nascent axon branches by either stabilizing or destabilizing nascent branches (Lewis et al., 2013). During axon morphogenesis, the majority of filopodia and nascent branches are retracted to maintain just a few that are consolidated into axon collaterals. It seems plausible, therefore, that axon branch retraction in developing neurons might involve molecular effectors that are also required for a distinct type of axon branch pruning. Based on our *in vitro* studies, we speculate that regulation of *de novo* protein synthesis could be the molecular process that is targeted in both axon branching and axon maintenance.

Based on our new findings, we suggest that Wnk as well as Nmnat are necessary components of axon branching as well as axon maintenance. Support for this model comes from the results of our genetic epistasis analysis. The loss of d*Wnk* during axon branching is only a problem if Sarm or Axed are present: in the absence of *Axed* (the most downstream effector of the destruction program in *Drosophila* known so far; Neukomm et al., 2017), loss of dWnk does not cause defects in axonal branching or maintenance. Implicit to this model is that dWnk is unlikely instructing axon branching but rather provides a safeguard function curbing destructive effectors such that retraction, pruning, or branch destruction can be restricted and constrained in a spatially restricted manner. A further implication of this model is the notion that loss of dWnk effectively represents a gain of function (on switch) of an axonal destruction program in developing axons.

In this context, it is also interesting to note that expression of Nmnat can compensate (i.e., rescue) for loss of dWnk in both axon branching and maintenance. It is well established that local depletion of Nmnat in adult neurons does directly lead to axon degeneration, i.e., has a role in axon maintenance independent of its developmental role (Milde et al., 2013). This is consistent with our new finding that post-developmental inactivation of dWnk or mammalian Wnk1/2 triggers axon degeneration.

Nmnat has been previously shown to protect from axon degeneration following axotomy by counter-acting Sarm-induced NAD+ depletion (Essuman et al., 2017; Sasaki et al., 2016; Yang et al., 2015; Gerdts et al., 2015) and Axed activity (Neukomm et al., 2017). We show in the present study that, even in the absence of axon injury, loss of Nmnat as well as loss of dWnk or overexpression of dSarm and Axed leads to progressive degeneration of adult mechanosensory axons without injury. This is consistent with previous reports showing that Nmnat loss in sensory neurons of the wing leads to spontaneous axon degeneration in adult flies (Fang et al., 2012) or that loss of NMNAT2 leads to truncation of peripheral nerve and CNS axon tracts in mice (Gilley et al., 2013). A role of Wnk1 in axon maintenance is also consistent with the finding that WNK function has been linked to a severe form of peripheral neuropathy (Lafreniere et al., 2004; Rivière et al., 2004; Roddier et al., 2005; Coen et al., 2006).

Our results, therefore, support the notion that both axon morphogenesis and maintenance require a constitutive involvement of Wnk and Nmnat.

A link between dWnk, Nmnat, and axon destructive factors is further corroborated by our biochemical experiments co-expressing these factors and using co-immunoprecipitations to analyze protein-protein interactions of dWnk or mammalian WNK1/2. First, our results suggest the possibility that dWnk, Nmnat, Sarm1, and Axed are able to form mixed complexes. Moreover, mammalian WNK1 can interact with WNK2 and Nmnat2 as well as SARM1. Although previous work has not identified Nmnat proteins as potential Wnk kinase substrates, our results suggest that this possibility is worthwhile to examine in future experiments. Second, whereas a vertebrate ortholog of Axed has not been described, we found that mammalian SARM1 overexpression strongly downregulates levels of WNK1, WNK2, NMNAT2, and NMNAT1. However, future experiments will have to confirm that this downregulation of proteins by Sarm1 is also occurring in neurons *in vivo*.

It has been reported that inhibition of axon degeneration can be accomplished by increasing or stabilizing levels of Nmnat protein (Babetto et al., 2013). Moreover, Highwire/Phr1, which is an additional conserved factor functioning in Wallerian degeneration, directly promotes the downregulation of Nmnat, and axon degeneration is strongly inhibited in Highwire/Phr1 mutants (Xiong et al., 2012). This previously described regulation of Nmnat levels is mediated via mitogen-activated protein kinase (MAPK) signaling and ubiquitin-dependent proteolysis. Our findings reported here suggest that Sarm1 may rather inhibit *de novo* protein synthesis in order to deplete Nmnat and other axon protective factors. Future studies will have to investigate in detail how the SARM1-dependent depletion of NAD+ also leads to a Wnk/Nmnat protein depletion as described here. Particularly interesting will be to determine how the destructive activity of Sarm protein can be limited during development to selective axon branch compartments in order to enable local axon branch pruning but prevent progressive axon degeneration.

Finally, Nmnat function has not only been involved in neuroprotection as a response to injury, such as axotomy, but also in a diverse range of neurodegenerative diseases, such as spinocerebellar ataxia (Zhai et al., 2008; Ruan et al., 2015), fronto-temporal dementia (FTD) and Parkinsonism (Ali et al., 2013), or glaucomatous optic neuropathy (Munemasa and Kitaoka, 2015), or following growth factor deprivation (Vohra et al., 2010). Future studies will need to consider the possibility that the newly identified dWnk and WNK1 and WNK2 kinases may also play similar neuroprotective roles in diverse types of neurodegenerative conditions.

STAR★METHODS

Detailed methods are provided in the online version of this paper and include the following:

- KEY RESOURCES TABLE
- RESOURCE AVAILABILITY

SUPPLEMENTAL INFORMATION

Supplemental information can be found online at https://doi.org/10.1016/j.neuron.2021.07.006.

ACKNOWLEDGMENTS

This work was supported by FWO (G077013N and G0B8919N to D.S.; G1214420N to G.E.-F.), VIB Belgium (D.S.), the Humboldt Foundation (D.S.), the Fondation pour la Recherche Medicale (AJE20141031276) and ERC Starting Grant (678302-NEUROMET) (J.C.), NINDS NS107483 (F.P.), an award from the Roger De Spoelberch Fondation (F.P.), and an award from the Thompson Family Foundation Initiative (F.P.). This work was performed within the framework of the LABEX CORTEX (ANR-11-LABX-0042/ANR-11-IDEX-0007). We thank our lab members for critical reading of the manuscript. Stocks obtained from the Bloomington Drosophila Stock Center (NIH P40OD018537) were used in this study. We thank M. Freeman, L. Neukomm, and T. Suzuki for sharing mutant fly stocks. We thank the personnel from the SCAR and ALECS-SPF mouse facility for animal care.

AUTHOR CONTRIBUTIONS

A.I., J.C., F.P., and D.S. designed the experiments and wrote the manuscript. A.I., D.A., S.V., M.P., D.D., Y.K., J.Y., and G.E.-F. conducted the developmental and Drosophila genetics experiments. J.C., D.M.V., S.H., L.M., and T.L. conducted the *in vivo* and *in vitro* mouse experiments. T.V., A.M., S.V., S.S., B.Y., M.-L.E., J.Y., and J.C. conducted molecular and cell culture work.

DECLARATION OF INTERESTS

The authors declare no competing interests.

Received: September 24, 2020
Revised: May 24, 2021
Accepted: July 8, 2021
Published: August 11, 2021

REFERENCES

Alessi, D.R., Zhang, J., Khanna, A., Hochdörfer, T., Shang, Y., and Kahle, K.T. (2014). The WNK-SPAK/OSR1 pathway: master regulator of cation-chloride cotransporters. Sci. Signal. *7*, re3.

Ali, Y.O., Li-Kroeger, D., Bellen, H.J., Zhai, R.G., and Lu, H.C. (2013). NMNATs, evolutionarily conserved neuronal maintenance factors. Trends Neurosci. *36*, 632–640.

Ali, Y.O., Allen, H.M., Yu, L., Li-Kroeger, D., Bakhshizadehmahmoudi, D., Hatcher, A., McCabe, C., Xu, J., Bjorklund, N., Taglialatela, G., et al. (2016). NMNAT2:HSP90 complex mediates proteostasis in proteinopathies. PLoS Biol. *14*, e1002472.

Anselmo, A.N., Earnest, S., Chen, W., Juang, Y.C., Kim, S.C., Zhao, Y., and Cobb, M.H. (2006). WNK1 and OSR1 regulate the Na+, K+, 2Cl- cotransporter in HeLa cells. Proc. Natl. Acad. Sci. USA *103*, 10883–10888.

Babetto, E., Beirowski, B., Russler, E.V., Milbrandt, J., and DiAntonio, A. (2013). The Phr1 ubiquitin ligase promotes injury-induced axon self-destruction. Cell Rep. *3*, 1422–1429.

Berg, S., Kutra, D., Kroeger, T., Straehle, C.N., Kausler, B.X., Haubold, C., Schiegg, M., Ales, J., Beier, T., Rudy, M., et al. (2019). ilastik: interactive machine learning for (bio)image analysis. Nat. Methods *16*, 1226–1232.

Berger, J., Senti, K.A., Senti, G., Newsome, T.P., Asling, B., Dickson, B.J., and Suzuki, T. (2008). Systematic identification of genes that regulate neuronal wiring in the Drosophila visual system. PLoS Genet. *4*, e1000085.

Chen, B.E., Kondo, M., Garnier, A., Watson, F.L., Püettmann-Holgado, R., Lamar, D.R., and Schmucker, D. (2006). The molecular diversity of Dscam is functionally required for neuronal wiring specificity in Drosophila. Cell *125*, 607–620.

Chen, C.Y., Lin, C.W., Chang, C.Y., Jiang, S.T., and Hsueh, Y.P. (2011). Sarm1, a negative regulator of innate immunity, interacts with syndecan-2 and regulates neuronal morphology. J. Cell Biol. *193*, 769–784.

Chia, P.H., Chen, B., Li, P., Rosen, M.K., and Shen, K. (2014). Local F-actin network links synapse formation and axon branching. Cell *156*, 208–220.

Coen, K., Pareyson, D., Auer-Grumbach, M., Buyse, G., Goemans, N., Claeys, K.G., Verpoorten, N., Laurà, M., Scaioli, V., Salmhofer, W., et al. (2006). Novel mutations in the HSN2 gene causing hereditary sensory and autonomic neuropathy type II. Neurology *66*, 748–751.

Coleman, M.P., and Freeman, M.R. (2010). Wallerian degeneration, wld(s), and nmnat. Annu. Rev. Neurosci. *33*, 245–267.

Conforti, L., Gilley, J., and Coleman, M.P. (2014). Wallerian degeneration: an emerging axon death pathway linking injury and disease. Nat. Rev. Neurosci. *15*, 394–409.

Costa, A.M., Pinto, F., Martinho, O., Oliveira, M.J., Jordan, P., and Reis, R.M. (2015). Silencing of the tumor suppressor gene WNK2 is associated with upregulation of MMP2 and JNK in gliomas. Oncotarget *6*, 1422–1434.

Courchet, J., Lewis, T.L., Jr., Lee, S., Courchet, V., Liou, D.Y., Aizawa, S., and Polleux, F. (2013). Terminal axon branching is regulated by the LKB1-NUAK1 kinase pathway via presynaptic mitochondrial capture. Cell *153*, 1510–1525.

Dascenco, D., Erfurth, M.L., Izadifar, A., Song, M., Sachse, S., Bortnick, R., Urwyler, O., Petrovic, M., Ayaz, D., He, H., et al. (2015). Slit and receptor tyrosine phosphatase 69D confer spatial specificity to axon branching via Dscam1. Cell *162*, 1140–1154.

Essuman, K., Summers, D.W., Sasaki, Y., Mao, X., DiAntonio, A., and Milbrandt, J. (2017). The SARM1 Toll/interleukin-1 receptor domain possesses intrinsic NAD^+ cleavage activity that promotes pathological axonal degeneration. Neuron *93*, 1334–1343.e5.

Fang, Y., Soares, L., Teng, X., Geary, M., and Bonini, N.M. (2012). A novel Drosophila model of nerve injury reveals an essential role of Nmnat in maintaining axonal integrity. Curr. Biol. *22*, 590–595.

Gagnon, K.B., England, R., and Delpire, E. (2006). Volume sensitivity of cation-Cl- cotransporters is modulated by the interaction of two kinases: Ste20-related proline-alanine-rich kinase and WNK4. Am. J. Physiol. Cell Physiol. *290*, C134–C142.

Gallolu, Kankanamalage, S., Karra, A.S., and Cobb, M.H. (2018). WNK pathways in cancer signaling networks. Cell Commun. Signal. *16*, 72.

Garrity, P.A., Lee, C.H., Salecker, I., Robertson, H.C., Desai, C.J., Zinn, K., and Zipursky, S.L. (1999). Retinal axon target selection in Drosophila is regulated by a receptor protein tyrosine phosphatase. Neuron *22*, 707–717.

Gerdts, J., Brace, E.J., Sasaki, Y., DiAntonio, A., and Milbrandt, J. (2015). SARM1 activation triggers axon degeneration locally via NAD^+ destruction. Science *348*, 453–457.

Gilley, J., and Coleman, M.P. (2010). Endogenous Nmnat2 is an essential survival factor for maintenance of healthy axons. PLoS Biol. *8*, e1000300.

Gilley, J., Adalbert, R., Yu, G., and Coleman, M.P. (2013). Rescue of peripheral and CNS axon defects in mice lacking NMNAT2. J. Neurosci. *33*, 13410–13424.

Hadchouel, J., Ellison, D.H., and Gamba, G. (2016). Regulation of renal electrolyte transport by WNK and SPAK-OSR1 kinases. Annu. Rev. Physiol. *78*, 367–389.

Hand, R., and Polleux, F. (2011). Neurogenin2 regulates the initial axon guidance of cortical pyramidal neurons projecting medially to the corpus callosum. Neural Dev. *6*, 30.

He, H., Kise, Y., Izadifar, A., Urwyler, O., Ayaz, D., Parthasarthy, A., Yan, B., Erfurth, M.L., Dascenco, D., and Schmucker, D. (2014). Cell-intrinsic requirement of Dscam1 isoform diversity for axon collateral formation. Science *344*, 1182–1186.

Hinz, U., Giebel, B., and Campos-Ortega, J.A. (1994). The basic-helix-loop-helix domain of Drosophila lethal of scute protein is sufficient for proneural function and activates neurogenic genes. Cell *76*, 77–87.

Hong, C., Moorefield, K.S., Jun, P., Aldape, K.D., Kharbanda, S., Phillips, H.S., and Costello, J.F. (2007). Epigenome scans and cancer genome sequencing converge on WNK2, a kinase-independent suppressor of cell growth. Proc. Natl. Acad. Sci. USA *104*, 10974–10979.

Hoopfer, E.D., McLaughlin, T., Watts, R.J., Schuldiner, O., O'Leary, D.D., and Luo, L. (2006). Wlds protection distinguishes axon degeneration following injury from naturally occurring developmental pruning. Neuron *50*, 883–895.

Hoorn, E.J., Nelson, J.H., McCormick, J.A., and Ellison, D.H. (2011). The WNK kinase network regulating sodium, potassium, and blood pressure. J. Am. Soc. Nephrol. *22*, 605–614.

Huppke, P., Wegener, E., Gilley, J., Angeletti, C., Kurth, I., Drenth, J.P.H., Stadelmann, C., Barrantes-Freer, A., Brück, W., Thiele, H., et al. (2019). Homozygous NMNAT2 mutation in sisters with polyneuropathy and erythromelalgia. Exp. Neurol. *320*, 112958.

Iascone, D.M., Li, Y., Sümbül, U., Doron, M., Chen, H., Andreu, V., Goudy, F., Blockus, H., Abbott, L.F., Segev, I., et al. (2020). Whole-neuron synaptic mapping reveals spatially precise excitatory/inhibitory balance limiting dendritic and somatic spiking. Neuron *106*, 566–578.e8.

Jun, P., Hong, C., Lal, A., Wong, J.M., McDermott, M.W., Bollen, A.W., Plass, C., Held, W.A., Smiraglia, D.J., and Costello, J.F. (2009). Epigenetic silencing of the kinase tumor suppressor WNK2 is tumor-type and tumor-grade specific. Neuro-oncol. *11*, 414–422.

Lafreniere, R.G., MacDonald, M.L., Dube, M.P., MacFarlane, J., O'Driscoll, M., Brais, B., Meilleur, S., Brinkman, R.R., Dadivas, O., Pape, T., et al. (2004). Identification of a novel gene (HSN2) causing hereditary sensory and autonomic neuropathy type II through the Study of Canadian Genetic Isolates. Am. J. Hum. Genet. *74*, 1064–1073.

Lewis, T.L., Jr., Courchet, J., and Polleux, F. (2013). Cell biology in neuroscience: cellular and molecular mechanisms underlying axon formation, growth, and branching. J. Cell Biol. *202*, 837–848.

Lewis, T.L., Jr., Turi, G.F., Kwon, S.K., Losonczy, A., and Polleux, F. (2016). Progressive decrease of mitochondrial motility during maturation of cortical axons in vitro and in vivo. Curr. Biol. *26*, 2602–2608.

Lukacs, M., Gilley, J., Zhu, Y., Orsomando, G., Angeletti, C., Liu, J., Yang, X., Park, J., Hopkin, R.J., Coleman, M.P., et al. (2019). Severe biallelic loss-of-function mutations in nicotinamide mononucleotide adenylyltransferase 2 (NMNAT2) in two fetuses with fetal akinesia deformation sequence. Exp. Neurol. *320*, 112961.

Matsuda, T., and Cepko, C.L. (2007). Controlled expression of transgenes introduced by in vivo electroporation. Proc. Natl. Acad. Sci. USA *104*, 1027–1032.

McCormick, J.A., and Ellison, D.H. (2011). The WNKs: atypical protein kinases with pleiotropic actions. Physiol. Rev. *91*, 177–219.

Meyer-Dilhet, G., and Courchet, J. (2020). In utero cortical electroporation of plasmids in the mouse embryo. STAR Protoc *1*, 100027.

Milde, S., Gilley, J., and Coleman, M.P. (2013). Subcellular localization determines the stability and axon protective capacity of axon survival factor Nmnat2. PLoS Biol. *11*, e1001539.

Moriguchi, T., Urushiyama, S., Hisamoto, N., Iemura, S., Uchida, S., Natsume, T., Matsumoto, K., and Shibuya, H. (2005). WNK1 regulates phosphorylation of cation-chloride-coupled cotransporters via the STE20-related kinases, SPAK and OSR1. J. Biol. Chem. *280*, 42685–42693.

Munemasa, Y., and Kitaoka, Y. (2015). Autophagy in axonal degeneration in glaucomatous optic neuropathy. Prog. Retin. Eye Res. *47*, 1–18.

Neukomm, L.J., Burdett, T.C., Seeds, A.M., Hampel, S., Coutinho-Budd, J.C., Farley, J.E., Wong, J., Karadeniz, Y.B., Osterloh, J.M., Sheehan, A.E., and Freeman, M.R. (2017). Axon death pathways converge on Axundead to promote functional and structural axon disassembly. Neuron *95*, 78–91.e5.

Osterloh, J.M., Yang, J., Rooney, T.M., Fox, A.N., Adalbert, R., Powell, E.H., Sheehan, A.E., Avery, M.A., Hackett, R., Logan, M.A., et al. (2012). dSarm/Sarm1 is required for activation of an injury-induced axon death pathway. Science *337*, 481–484.

Pela, I. (2012). Familial hyperkalemic hypertension: a new early-onset pediatric case. Clin. Pediatr. Endocrinol. *21*, 5–9.

Pfeiffer, B.D., Jenett, A., Hammonds, A.S., Ngo, T.T., Misra, S., Murphy, C., Scully, A., Carlson, J.W., Wan, K.H., Laverty, T.R., et al. (2008). Tools for neuroanatomy and neurogenetics in Drosophila. Proc. Natl. Acad. Sci. USA *105*, 9715–9720.

Polleux, F., and Ghosh, A. (2002). The slice overlay assay: a versatile tool to study the influence of extracellular signals on neuronal development. Sci. STKE *2002*, pl9.

Raff, M.C., Whitmore, A.V., and Finn, J.T. (2002). Axonal self-destruction and neurodegeneration. Science *296*, 868–871.

Rafiqi, F.H., Zuber, A.M., Glover, M., Richardson, C., Fleming, S., Jovanović, S., Jovanović, A., O'Shaughnessy, K.M., and Alessi, D.R. (2010). Role of the WNK-activated SPAK kinase in regulating blood pressure. EMBO Mol. Med. *2*, 63–75.

Rahmani, B., Fekrmandi, F., Ahadi, K., Ahadi, T., Alavi, A., Ahmadiani, A., and Asadi, S. (2018). A novel nonsense mutation in WNK1/HSN2 associated with sensory neuropathy and limb destruction in four siblings of a large Iranian pedigree. BMC Neurol. *18*, 195.

Richardson, C., and Alessi, D.R. (2008). The regulation of salt transport and blood pressure by the WNK-SPAK/OSR1 signalling pathway. J. Cell Sci. *121*, 3293–3304.

Richardson, C., Rafiqi, F.H., Karlsson, H.K., Moleleki, N., Vandewalle, A., Campbell, D.G., Morrice, N.A., and Alessi, D.R. (2008). Activation of the thiazide-sensitive Na+-Cl- cotransporter by the WNK-regulated kinases SPAK and OSR1. J. Cell Sci. *121*, 675–684.

Rivière, J.B., Verlaan, D.J., Shekarabi, M., Lafrenière, R.G., Bénard, M., Der Kaloustian, V.M., Shbaklo, Z., and Rouleau, G.A. (2004). A mutation in the HSN2 gene causes sensory neuropathy type II in a Lebanese family. Ann. Neurol. *56*, 572–575.

Roddier, K., Thomas, T., Marleau, G., Gagnon, A.M., Dicaire, M.J., St-Denis, A., Gosselin, I., Sarrazin, A.M., Larbrisseau, A., Lambert, M., et al. (2005). Two mutations in the HSN2 gene explain the high prevalence of HSAN2 in French Canadians. Neurology *64*, 1762–1767.

Rual, J.F., Ceron, J., Koreth, J., Hao, T., Nicot, A.S., Hirozane-Kishikawa, T., Vandenhaute, J., Orkin, S.H., Hill, D.E., van den Heuvel, S., and Vidal, M. (2004). Toward improving Caenorhabditis elegans phenome mapping with an ORFeome-based RNAi library. Genome Res. *14* (10B), 2162–2168.

Ruan, K., Zhu, Y., Li, C., Brazill, J.M., and Zhai, R.G. (2015). Alternative splicing of Drosophila Nmnat functions as a switch to enhance neuroprotection under stress. Nat. Commun. *6*, 10057.

Sachse, S.M., Lievens, S., Ribeiro, L.F., Dascenco, D., Masschaele, D., Horré, K., Misbaer, A., Vanderroost, N., De Smet, A.S., Salta, E., et al. (2019). Nuclear import of the DSCAM-cytoplasmic domain drives signaling capable of inhibiting synapse formation. EMBO J. *38*, e99669.

Sasaki, Y., Nakagawa, T., Mao, X., DiAntonio, A., and Milbrandt, J. (2016). NMNAT1 inhibits axon degeneration via blockade of SARM1-mediated NAD^+ depletion. eLife *5*, e19749.

Sato, A., and Shibuya, H. (2018). Glycogen synthase kinase 3ß functions as a positive effector in the WNK signaling pathway. PLoS ONE *13*, e0193204.

Schneider, C.A., Rasband, W.S., and Eliceiri, K.W. (2012). NIH Image to ImageJ: 25 years of image analysis. Nat. Methods *9*, 671–675.

Shekarabi, M., Girard, N., Rivière, J.B., Dion, P., Houle, M., Toulouse, A., Lafrenière, R.G., Vercauteren, F., Hince, P., Laganiere, J., et al. (2008). Mutations in the nervous system–specific HSN2 exon of WNK1 cause hereditary sensory neuropathy type II. J. Clin. Invest. *118*, 2496–2505.

Shekarabi, M., Zhang, J., Khanna, A.R., Ellison, D.H., Delpire, E., and Kahle, K.T. (2017). WNK kinase signaling in ion homeostasis and human disease. Cell Metab. *25*, 285–299.

Siew, K., and O'Shaughnessy, K.M. (2013). Extrarenal roles of the with-no-lysine[K] kinases (WNKs). Clin. Exp. Pharmacol. Physiol. *40*, 885–894.

Srahna, M., Leyssen, M., Choi, C.M., Fradkin, L.G., Noordermeer, J.N., and Hassan, B.A. (2006). A signaling network for patterning of neuronal connectivity in the Drosophila brain. PLoS Biol. *4*, e348.

Sudarsanam, S., Yaniv, S., Meltzer, H., and Schuldiner, O. (2020). Cofilin regulates axon growth and branching of *Drosophila* γ-neurons. J. Cell Sci. *133*, jcs232595.

Südhof, T.C. (2017). Molecular neuroscience in the 21st century: a personal perspective. Neuron *96*, 536–541.

Urwyler, O., Izadifar, A., Dascenco, D., Petrovic, M., He, H., Ayaz, D., Kremer, A., Lippens, S., Baatsen, P., Guérin, C.J., and Schmucker, D. (2015). Investigating CNS synaptogenesis at single-synapse resolution by combining reverse genetics with correlative light and electron microscopy. Development *142*, 394–405.

Urwyler, O., Izadifar, A., Vandenbogaerde, S., Sachse, S., Misbaer, A., and Schmucker, D. (2019). Branch-restricted localization of phosphatase Prl-1 specifies axonal synaptogenesis domains. Science *364*, eaau9952.

Veríssimo, F., and Jordan, P. (2001). WNK kinases, a novel protein kinase subfamily in multi-cellular organisms. Oncogene *20*, 5562–5569.

Vidal-Petiot, E., Elvira-Matelot, E., Mutig, K., Soukaseum, C., Baudrie, V., Wu, S., Cheval, L., Huc, E., Cambillau, M., Bachmann, S., et al. (2013). WNK1-related familial hyperkalemic hypertension results from an increased expression of L-WNK1 specifically in the distal nephron. Proc. Natl. Acad. Sci. USA *110*, 14366–14371.

Vitari, A.C., Deak, M., Morrice, N.A., and Alessi, D.R. (2005). The WNK1 and WNK4 protein kinases that are mutated in Gordon's hypertension syndrome phosphorylate and activate SPAK and OSR1 protein kinases. Biochem. J. *391*, 17–24.

Vohra, B.P., Sasaki, Y., Miller, B.R., Chang, J., DiAntonio, A., and Milbrandt, J. (2010). Amyloid precursor protein cleavage-dependent and -independent axonal degeneration programs share a common nicotinamide mononucleotide adenylyltransferase 1-sensitive pathway. J. Neurosci. *30*, 13729–13738.

Wen, Y., Parrish, J.Z., He, R., Zhai, R.G., and Kim, M.D. (2011). Nmnat exerts neuroprotective effects in dendrites and axons. Mol. Cell. Neurosci. *48*, 1–8.

Wilson, F.H., Disse-Nicodème, S., Choate, K.A., Ishikawa, K., Nelson-Williams, C., Desitter, I., Gunel, M., Milford, D.V., Lipkin, G.W., Achard, J.M., et al. (2001). Human hypertension caused by mutations in WNK kinases. Science *293*, 1107–1112.

Wu, A., Wolley, M., and Stowasser, M. (2019). The interplay of renal potassium and sodium handling in blood pressure regulation: critical role of the WNK-SPAK-NCC pathway. J. Hum. Hypertens. *33*, 508–523.

Xiong, X., Hao, Y., Sun, K., Li, J., Li, X., Mishra, B., Soppina, P., Wu, C., Hume, R.I., and Collins, C.A. (2012). The Highwire ubiquitin ligase promotes axonal degeneration by tuning levels of Nmnat protein. PLoS Biol. *10*, e1001440.

Xu, B., English, J.M., Wilsbacher, J.L., Stippec, S., Goldsmith, E.J., and Cobb, M.H. (2000). WNK1, a novel mammalian serine/threonine protein kinase lacking the catalytic lysine in subdomain II. J. Biol. Chem. *275*, 16795–16801.

Yang, C.L., Angell, J., Mitchell, R., and Ellison, D.H. (2003). WNK kinases regulate thiazide-sensitive Na-Cl cotransport. J. Clin. Invest. *111*, 1039–1045.

Yang, J., Wu, Z., Renier, N., Simon, D.J., Uryu, K., Park, D.S., Greer, P.A., Tournier, C., Davis, R.J., and Tessier-Lavigne, M. (2015). Pathological axonal death through a MAPK cascade that triggers a local energy deficit. Cell *160*, 161–176.

Yuan, J.H., Hashiguchi, A., Yoshimura, A., Sakai, N., Takahashi, M.P., Ueda, T., Taniguchi, A., Okamoto, S., Kanazawa, N., Yamamoto, Y., et al. (2017). WNK1/HSN2 founder mutation in patients with hereditary sensory and autonomic neuropathy: A Japanese cohort study. Clin. Genet. *92*, 659–663.

Zhai, R.G., Zhang, F., Hiesinger, P.R., Cao, Y., Haueter, C.M., and Bellen, H.J. (2008). NAD synthase NMNAT acts as a chaperone to protect against neurodegeneration. Nature *452*, 887–891.

STAR★METHODS

KEY RESOURCES TABLE

REAGENT or RESOURCE	SOURCE	IDENTIFIER
Antibodies		
Rabbit anti-GFP	Invitrogen	Cat# A-11122; RRID:AB_221569
Mouse anti-GFP	Abcam	Cat# ab1218; RRID:AB_298911
Rabbit anti-DsRed	Takara Bio	Cat# 632496; RRID:AB_10013483
Mouse anti-Fasciclin II (FasII) ID4	Developmental Studies Hybridoma Bank (DSHB)	RRID:AB_528235
Rat anti-N-Cadherin	Developmental Studies Hybridoma Bank (DSHB)	RRID:AB_528121
Guinea Pig anti-Wnk	This paper, Schmucker lab	N/A
Alexa Fluor 488 goat anti-rabbit IgG (H+L)	Invitrogen	Cat# A-11034; RRID:AB_2576217
Alexa Fluor 488 goat anti-mouse IgG (H+L)	Invitrogen	Cat# A-11029; RRID:AB_138404
Alexa Fluor 555 goat anti-rabbit IgG (H+L)	Invitrogen	Cat# A-21429; RRID:AB_2535850
Alexa Fluor 488 Goat anti-Guinea Pig IgG (H+L)	Invitrogen	Cat# A-11073; RRID:AB_2534117
Alexa Fluor 647 Goat anti-Guinea Pig IgG (H+L)	Invitrogen	Cat# A-21450; RRID:AB_141882
Chicken polyclonal anti-GFP	Aves Lab	Cat# GFP-1020; RRID:AB_10000240
Rabbit polyclonal anti-RFP	Abcam	Cat# Ab124754; RRID:AB_10971665
Rabbit polyclonal anti-CUX1 (M-222)	Santa Cruz	Cat# Sc-13024; RRID:AB_2261231
Rat anti-HA High Affinity	Roche	Cat# 11867423001; RRID:AB_390918
Rabbit anti-p44/42 MAPK (Erk1/2)	Cell Signaling Technology	Cat# 9102S; RRID:AB_330744
Alexa Fluor 488 Goat anti-Chicken IgY (H+L)	Invitrogen	Cat# A-11039; RRID:AB_142924
Alexa Fluor 546 Goat anti-Rabbit IgG (H+L)	Invitrogen	Cat# A-11010; RRID:AB_2534077
Peroxidase AffiniPure Donkey Anti-Rabbit IgG (H+L)	Jackson ImmunoResearch	Cat# 711-035-152; RRID:AB_10015282
Peroxidase AffiniPure Donkey Anti-Rat IgG (H+L)	Jackson ImmunoResearch	Cat# 712-035-153; RRID:AB_2340639
Rabbit anti-FLAG	Sigma-Aldrich	Cat# F7425; RRID:AB_439687
Mouse anti-V5	Sigma-Aldrich	Cat# V8012; RRID:AB_261888
Rabbit anti-myc	Abcam	Cat# ab9106; RRID:AB_307014
Rabbit anti-tubulin	Novus Biologicals	Cat# NB600-936; RRID:AB_10000656
Peroxidase AffiniPure Goat Anti-Rat IgG (H+L)	Jackson ImmunoResearch	Cat# 112-035-003; RRID:AB_2338128
Peroxidase AffiniPure Goat Anti-Rabbit IgG (H+L)	Jackson ImmunoResearch	Cat# 111-035-144; RRID:AB_2307391
Peroxidase AffiniPure Goat Anti-Mouse IgG (H+L)	Jackson ImmunoResearch	Cat# 115-035-003; RRID:AB_10015289
Peroxidase AffiniPure Goat Anti-Guinea Pig IgG (H+L)	Jackson ImmunoResearch	Cat# 106-035-003; RRID:AB_2337402
Chemicals, peptides, and recombinant proteins		
Fetal Bovine Serum	Gemini Bio-Products	Cat# 100-500
B-27 Supplement (50x)	Fisher Scientific	Cat# A3582801
N-2 Supplement (100x)	Thermo Fisher Scientific	Cat# 17502048
GlutaMAX Supplement	Thermo Fisher Scientific	Cat# 35050061
Neurobasal Medium	Thermo Fisher Scientific	Cat# 21103049
Hanks' Balance Salt Solution (HBSS), calcium, magnesium, no phenol red	Thermo Fisher Scientific	Cat# 14-025-076
Penicillin/Streptomycin	Thermo Fischer Scientific	Cat# 15140-122
Papain	Worthington	Cat# LK003178
DNase I	Sigma-Aldrich	Cat# D5025
Poly-d-Lysine	Thermo Fischer Scientific	Cat# A3890401
Fast Green FCF	Sigma-Aldrich	Cat# F7252-5G

(*Continued on next page*)

Continued

REAGENT or RESOURCE	SOURCE	IDENTIFIER
DAPI Fluoromount-G	Southern Biotech	Cat# 0100-20
32% Paraformaldehyde Aqueous Solution, EM Grade	Electron Microscopy Sciences	Cat# 15614-S
Glutaraldehyde 25% Aqueous Solution	Electron Microscopy Sciences	Cat# 16220
Tamoxifen, > 99%	Sigma-Aldrich	Cat# T5648-1G
Corn Oil	Sigma-Aldrich	Cat# C8267-500ML
HOECHST 33258	Thermo scientific	Cat# 62249
DiD	Invitrogen	Cat# D7757
DMEM/F-12	GIBCO	Cat# 11320033
DMEM	GIBCO	Cat# 11966025
Fetal Bovine Serum	GIBCO	Cat# A4766801
Fetal Bovine Serum, heat inactivated	GIBCO	Cat# 10082147
L-Glutamine	GIBCO	Cat# 25030149
GENIUS DNA Transfection Reagent	Westburg	Cat# WB 7-1050
Cycloheximide	Sigma-Aldrich	Cat# C7698
Schneider's Insect Medium	Sigma-Aldrich	Cat# S0146
Blasticidin	Invitrogen	Cat# A1113903
Copper Sulfate	Sigma-Aldrich	Cat# PHR1477
PBS	GIBCO	Cat# 10010023
TWEEN® 20	Sigma-Aldrich	Cat# 9005-64-5
Halt Protease and Phosphatase Inhibitor Cocktail (100X)	Thermo scientific	Cat# 78440
Blotting-Grade Blocker	Biorad	Cat# 1706404
Bovine Serum Albumin	Sigma-Aldrich	Cat# A7030
Pierce ECL Western Blotting Substrate	Thermo scientific	Cat# 32106
Pierce ECL Plus Western Blotting Substrate	Thermo scientific	Cat# 32134
Pierce Anti-c-Myc Magnetic Beads	Thermo scientific	Cat# 88842
Pierce Anti-HA Magnetic Beads	Thermo scientific	Cat# 88837
Anti-V5-tag mAb-Magnetic Beads (Monoclonal Antibody)	MBL	Cat# M167-11
In-Fusion HD Cloning Kit	Clontech	Cat# 639649
Dynabeads Antibody Coupling kit	Invitrogen	Cat# 14311D
Amaxa® Cell Line Nucleofector® Kit V	Lonza	Cat# VCA-1003
Experimental models: Cell lines		
SH-SY5Y	ATCC	Cat# CRL-2266
HEK293T	ATCC	Cat# CRL-3216
S2	DGRC	stock #181
Experimental models: Organisms/strains		
Mouse F1 hybrid (C57BL/6J x 129/SvJ)	Mice, Polleux Lab, Charles River Labs	N/A; Strain Code: 027
UAS-Wnk RNAi	Drosophila stock Center Bloomington BDSC	RRID:BDSC_62150
UAS-Wnk RNAi	Drosophila stock Center Vienna VDRC	RRID:VDRCID_102654
pnr-Gal4	BDSC	RRID:BDSC_25758
Elav-Gal4	BDSC	RRID:BDSC_458
hsFLP, UAS-mCD8-GFP	BDSC	RRID:BDSC_28832
Wnk^{G1286}	Berger et al., 2008	N/A
Wnk^{F1183}	Berger et al., 2008	N/A
Wnk^{G1286} *FRT80B*	This paper	N/A
Wnk^{F1183} *FRT80B*	This paper	N/A
FRT80B Tub-Gal80	BDSC	RRID:BDSC_5191

(*Continued on next page*)

Continued

REAGENT or RESOURCE	SOURCE	IDENTIFIER
UAS-Wnk^{WT}	This paper	N/A
FRT80B	BDSC	RRID:BDSC_1988
DC1.4-Flp	Pfeiffer et al., 2008	N/A
CantonS	BDSC	RRID:BDSC_64349
20xUAS-FRT- STOP-FRT-CD8GFP-2A-syt-mCherry	Garrity et al., 1999	N/A
UAS-NmnatRNAi	BDSC	RRID:BDSC_29402
NMNAT^{2} FRT82B	(Neukomm et al., 2017), Freeman lab	N/A
FRT82B	BDSC	RRID:BDSC_2035
5xUAS-axed^{long}	(Neukomm et al., 2017), Freeman lab	N/A
5xUAS-dSarm^{WT}	(Neukomm et al., 2017), Freeman lab	N/A
UAS-Nmnat-HA	BDSC	RRID:BDSC_39702
UAS-Axed RNAi	BDSC	RRID:BDSC_58220
455-Gal4	Hinz et al., 1994	N/A
R15E08-Gal4	Pfeiffer et al., 2008	N/A
UAS-Wnk-EYFP	This paper	N/A
P{QUAS-mCD8-GFP.P}5J	BDSC	RRID:BDSC_30003
Gr21a-GAL4.C	BDSC	RRID:BDSC_23890
Or88a-GAL4.F	BDSC	RRID:BDSC_23137
ato-Gal4-14a	(Srahna et al., 2006), Hassan lab	N/A
ato-Gal4.3.6-10	(Srahna et al., 2006), Hassan lab	N/A
hsFLP, tubP-GAL80, FRT19A	BDSC	RRID:BDSC_5134
FRT19A	BDSC	RRID:BDSC_1744
UAS-Fray RNAi	BDSC	RRID:BDSC_42569
UAS-Kcc RNAi	BDSC	RRID:BDSC_34584
UAS-dSarm RNAi	BDSC	RRID:BDSC_31175
UAS-Wnk$^{kinase\ dead}$	This paper	N/A
Recombinant DNA		
Plasmid: pCAG-TdTomato	Lewis et al., 2016	N/A
Plasmid: pLKO.1	The RNAi Consortium shRNA Library; OpenBioSystems	Cat#UN3245
Plasmid: pLKO-shWNK1-TRC0000027035	The RNAi Consortium shRNA Library; OpenBioSystems	RMM3981-201757342
Plasmid: pLKO-shWNK1-TRC0000027039	The RNAi Consortium shRNA Library; OpenBioSystems	RMM3981-201757346
Plasmid: pLKO-shWNK2-TRC0000027606	The RNAi Consortium shRNA Library; OpenBioSystems	RMM3981-201757913
Plasmid: pLKO-shWNK2-TRC0000027661	The RNAi Consortium shRNA Library; OpenBioSystems	RMM3981-201757968
Plasmid: pLKO-shWNK2-TRC0000027668	The RNAi Consortium shRNA Library; OpenBioSystems	RMM3981-201757975
Plasmid: pCAG-CreON-WNK1-27035	This paper	N/A
Plasmid: pCAG-CreON-WNK1-27039	This paper	N/A
Plasmid: pCAG-CreON-WNK2-27661	This paper	N/A
Plasmid: pCAG-CreON-WNK2-27668	This paper	N/A
Plasmid: pCAG-ERT2CreERT2	Matsuda and Cepko, 2007	Addgene Plasmid #13777
Plasmid: pCIG2-HA-WNK1	This paper	N/A
Plasmid: pSCV2 (pCAG-mVenus)	Hand and Polleux, 2011	N/A
Plasmid: pCMV-myc-WNK1	Xu et al., 2000	Addgene Plasmid #38779
Plasmid: pCDNA3-WNK2-V5	Chen et al., 2011	Addgene Plasmid #24569
Plasmid: pUASattB-dWnk	This paper	N/A

(*Continued on next page*)

Continued

REAGENT or RESOURCE	SOURCE	IDENTIFIER
Plasmid: pUASattB-Axed	This paper	N/A
Plasmid: pMT-V5-Axed	This paper	N/A
Plasmid: pCDNA5-NMNAT1-EYFP-FLAG	This paper	N/A
Plasmid: pCDNA5-NMNAT2-EYFP-FLAG	This paper	N/A
Plasmid: pCDNA5-SARM1-ECFP-HA	This paper	N/A
Plasmid: pCDNA5-SARM1-ΔTIR-ECFP-HA	This paper	N/A
Plasmid: pCDNA5-turboGFP	This paper	N/A
Plasmid: pCMV-FLAG-NMNAT2	Gilley and Coleman, 2010	N/A
Plasmid: pCMV-FLAG-WldS	Gilley and Coleman, 2010	N/A
Software and algorithms		
Ilastik: density counter	Berg et al., 2019	https://www.ilastik.org/
FIJI is a modified ImageJ distribution	Schneider et al., 2012	https://imagej.nih.gov/ij/
GraphPad PRISM	GraphPad Software Inc.	https://www.graphpad.com/scientific-software/prism/
NIS-Elements	Nikon	https://www.microscope.healthcare.nikon.com/products/software/nis-elements
A1R Confocal Microscope	Nikon	https://www.microscope.healthcare.nikon.com/products/confocal-microscopes/a1hd25-a1rhd25
LSM 710 confocal microscope	Zeiss	https://www.zeiss.com/microscopy/int/products/confocal-microscopes.html
LSM 780 confocal microscope	Zeiss	https://www.zeiss.com/microscopy/int/products/confocal-microscopes.html
ProteinSimple FluorChemQ imaging system	ProteinSimple	https://www.proteinsimple.com/fluorchem_m.html
Chemi-Doc_IT imager	UVP	https://www.uvp.com/products/

RESOURCE AVAILABILITY

Lead contact

Further information and requests for resources and reagents may be directed to and will be fulfilled by the Lead Contact, Dr. Dietmar Schmucker (dslab@uni-bonn.de).

Materials availability

Fly strains and expression constructs generated in this study are available from the Lead Contact upon request. Plasmids can be obtained with a completed Materials Transfer Agreement as requested by Flanders Institute of Biotechnology (VIB).

Data and code availability

All relevant data supporting the findings of this study are listed in Key resources table or are available from the Lead Contact upon request.

This paper does not report original code

Any additional information required to reanalyze the data reported in this paper is available from the lead contact upon request.

EXPERIMENTAL MODEL AND SUBJECT DETAILS

Flies (*D. melanogaster*) genotypes for all experiments and all figure panels are listed in Table S1. For all genetic crosses males and female flies were used. UAS-RNAi lines were obtained from the Vienna *Drosophila* Resource Center (Vienna, Austria) or from the Bloomington *Drosophila* stock center (Indiana University, USA). All crosses were performed at 25°C, except for late knock-down of dWnk, for which a shift from 18°C to 29°C at late-pupal stage (after axon branching had already occurred) was used to prevent RNAi activation during development, and the presence of normal axon morphologies was confirmed in young adult control flies. Single-cell labeling and transgene expression were performed as described (Urwyler et al., 2019). For analysis of axon branch patterns of dye-labeled mechanosensory neurons at adult stages only VNCs of female animals were used in order to avoid variability due to size differences of male and female flies. In all other experiments male and female animals were used.

Mice were used according to protocols approved by the Institutional Animal Care and Use Committee at Columbia University Medical School and the Ethics committee of the University of Lyon, and in accordance with National Institutes of Health guidelines and the French and European Union legislation. All animals were maintained in a 12-hour light/dark cycle. We crossed C57BL/6J males with 129/SvJ females to generate F1 hybrids (C57BL/6J x 129/SvJ). Time-pregnant F1 hybrid females were obtained by overnight breeding with C57BL/6J males. Noon following breeding was considered E0.5. Embryos of both sexes were used in electroporation procedures. Electroporations were performed at developmental stage E15.5. Mice were sacrificed at the age indicated in the figures.

METHOD DETAILS

Plasmids and molecular cloning

Empty vector pLKO.1 and shRNA targeting plasmids toward mouse WNK1 (TRC0000027035 and TRC0000027039) or mouse WNK2 (TRC0000027606, TRC0000027661 and TRC0000027668) were selected from The RNAi Consortium shRNA Library (TRC) from the Broad Institute and purchased from OpenBioSystems. Unless stated otherwise shRNA plasmids targeting a same gene were pooled at a 1:1 (WNK1) or 1:1:1 (WNK2) ratio and used at the final concentration of 1 mg/mL for in utero cortical electroporation or *ex vivo* electroporation. The CreON-shWNK plasmids were synthesized (Vigene) using these same shRNA targeting sequences under a CMV promoter. The CMV promoter was then replaced with a CMV enhancer/chicken β-Actin promoter (CAG) sing PCR amplification and InFusion cloning (Clonetech). pCAG-ERT2CreERT2 has been described previously (Matsuda and Cepko, 2007) and was purchased via Addgene (Addgene #13777).

Plasmids containing rat myc-WNK1, human WNK2-V5, and mouse SARM1 were a gift from Melanie Cobb, Joseph Costello, and Yi-Ping Hsueh, respectively (Addgene plasmid #38779, #24569, and #50707) (Xu et al., 2000; Chen et al., 2011; Hong et al., 2007). The mVenus expressing vector pSCV2 was described previously (Hand and Polleux, 2011). Human NMNAT1 and NMNAT2 were PCR amplified from clone HsCD00353283 and HsCD00399665 from the DNASU plasmid repository. dWnk and Axed were amplified from *Drosophila* cDNA and cloned into pUASTattB using Gibson Assembly (NEB E2611S). In order to create a stable *Drosophila* cell line, Axed was additionally subcloned into pMT-V5-His A (Thermo Scientific) using Gibson Assembly, and pCoBlast (Thermo Scientific) was used as a selection vector. All expression vectors used for cell line transfections were further constructed using the Gateway cloning system (Life Technologies). In brief, NMNAT1, NMNAT2, and SARM1 open reading frames were amplified by PCR adding a 5′ attB1 site and a mammalian Kozak sequence in the forward primer, as well as a 3′ attB2 sequence in the reverse primer. SARM1ΔTIR was generated by amplifying solely the N-terminal SARM1, excluding the 165 amino acids at the C-terminal comprising the TIR (Toll/Interleukin-1 Receptor) domain. The stop codon was removed to allow in-frame C-terminal tagging. In a similar manner, turboGFP (GFP) was amplified with the retention of the stop codon to use as a transfection control. The amplicons were subcloned into a modified version of pDONR223 (Rual et al., 2004) by a BP transferase reaction. Subsequently, an LR reaction was performed according to the manufacturer's instructions with pcDNA5FRT-TO-GW-EYFP-FLAG and pcDNA5FRT-TO-GW-ECFP-HA destination vectors to generate NMNAT1-EYFP-FLAG, NMNAT2-EYFP-FLAG, SARM1-ECFP-HA, and SARM1ΔTIR -ECFP-HA. Finally, pCMV-FLAG-NMNAT2 and pCMV-FLAG-WldS were a gift of the Coleman lab.

Cell cultures and transfections

Primary neuronal cultures were performed as described previously (Polleux and Ghosh, 2002). Mouse cortices were dissected in Hank's Buffered Salt Solution (HBSS) supplemented with 2.5 mM HEPES, 1 mM $CaCl_2$ (Sigma), 1 mM $MgSO_4$ (Sigma), 4 mM $NaHCO_3$ (Sigma) and 30 mM D-glucose (Sigma), hereafter referred to as cHBSS. Cortices were dissociated in cHBSS containing papain (Worthington) and DNase I (100 μg/mL, Sigma) for 20 min at 37°C, washed three times and manually triturated in cHBSS supplemented with DNase. Cells were then plated at 7.5×10^4 cells per 35 mm glass bottom dish (Matek) coated with 1 mg/mL poly-D-lysine (Sigma) and cultured for 5, 10, 15 or 20 days in Neurobasal medium supplemented with 1x B27, 1x N2, 2 mM L-glutamine and 5 units/mL penicillin- 50 mg/mL streptomycin.

SH-SY5Y cells (ATCC, CRL-2266) and HEK293T cells (ATCC, CRL-3216) were cultured in DMEM/F12 and DMEM, respectively, supplemented with 10% FBS, 2 mM L-Glutamine and 100 units/mL penicillin- 100 μg/mL streptomycin. Cell transfection were performed in 6-well plates using GENIUS DNA transfection reagent with 2 μg of each plasmid. Unless otherwise indicated, all products for cell cultures were obtained from Invitrogen/Life Technologies. For cycloheximide (CHX) experiments, HEK293T cells were treated with the inhibitor at 100 μg/mL starting 24 hours after transfection. Protein lysates were prepared at t = 0 (no CHX treatment) and at 2, 4 and 6 hours of CHX treatment.

Drosophila S2 cells were obtained from DGRC and grown in Schneiders medium supplemented with 10% HI FBS and 100 units/mL penicillin- 100 μg/mL streptomycin (Invitrogen/Life Technologies). The stable cell line expressing Axed-V5 was grown in the presence of blasticidin (Life Technologies). Expression was induced using 500 μM $CuSO_4$. Cells were transfected using the Amaxa Nucleofector II device (Lonza) with 1 to 2 μg of DNA (solution V, program D023).

Ex utero and in utero cortical electroporations

Ex utero electroporation of mouse dorsal telencephalic progenitors was performed as previously described (Courchet et al., 2013) by injecting plasmid DNA (1-2 μg/μL endotoxin-free plasmid DNA, Midi prep kit from Macherey-Nagel) plus 0.5% Fast Green (1:20 ratio, Sigma) using the picospritzer III (Parker) microinjector into the lateral ventricles of isolated E15.5 embryonic heads that were

decapitated and placed in complete HBSS (Polleux and Ghosh, 2002). Electroporations were performed on the whole head (skin and skull intact) with gold-coated electrodes (GenePads 5 × 7 mm BTX) using an ECM 830 electroporator (BTX) and the following parameters: five 100 ms long pulses separated by 100 ms long intervals at 20 V. Immediately after electroporation, cortices were prepared for primary neuronal culture.

Protocol for in utero electroporation is fully described in Meyer-Dilhet and Courchet (2020). We used timed-pregnant F1 females from C57BL/6J X 129/SvJ crosses (The Jackson Laboratory). Electroporation was performed at E15.5 to target progenitors generating cortical layer 2/3 PNs. The electroporation settings were: 4 pulses of 45 V for 50 ms with 500 ms interval. Electroporated mice were sacrificed at the indicated ages.

Immunoprecipitations

Immunoprecipitations were performed as described before (Sachse et al., 2019). Briefly, SH-SY5Y or HEK293T cells were harvested 24 to 48 hours after transfections in ice-cold 1x PBS and lysed in RIPA buffer (25 mM Tris pH 7.6, 150 mM NaCl, 1% sodiumdeoxycholate, 0.5% NP-40, 1% SDS, 0.5% Triton X-100, 5% glycerol) containing Halt protease and phosphatase inhibitor cocktail (Pierce). Input extracts were cleared by centrifugation and tagged proteins were precipitated for one hour at RT followed by extensive washing in RIPA buffer or TBS-Tween. For immunoprecipitation, we used the following magnetic beads: mouse anti-c-*myc*, mouse anti-HA (both Pierce), and mouse anti-HA (MBL). Following precipitations, protein complexes were heat-eluted in SDS sample buffer or 0.1M glycine.

Immunoprecipitation in S2 cells was performed 48 hours after the induction of the stable S2 cell line expressing Axed-V5. Induction was carried out 6 or 24 hours after transfection with the plasmid containing dWnk. Cells were harvested in RIPA buffer supplemented with protease and phosphatase inhibitors and proteins were precipitated for two hours at RT. The The Dynabeads Antibody Coupling kit (Invitrogen) was used to coat 3 mg beads with the custom-made dWnk antibody. 1 mg beads were used for the mock IP. Coupling of the antibody to the beads was carried out at 37°C overnight.

Western blotting

Denaturated protein samples were submitted to SDS-PAGE and transferred to polyvinylidene difluoride (PVDF) or nitrocellulose membranes (Biorad). Primary antibody incubation was performed overnight at 4°C using the appropriate antibody diluted in TBS-Tween (0.1%) containing 5% milk or BSA. HRP-conjugated secondary antibodies were incubated at room temperature for 1 to 2 hours in in TBS-Tween with milk or BSA. Protein bands were visualized with a ProteinSimple FluorChemQ imaging system or Chemi-Doc_IT imager (UVP) using ECL reagent (Pierce). Three or more independent experiments were performed for all immunoblotting data.

Dye labeling of *Drosophila* mechanosensory neuron axons

Dye fills were performed as described previously (Chen et al., 2006). Adult flies were glued to an insect pin (Fine Science Tools, #26000-25) and large mechanosensory bristles on the dorsal thorax were plucked manually with forceps. Flies were subsequently beheaded, their abdomen opened and fixed overnight at 4°C in 3.7% (w/v) paraformaldehyde (Electron Microscopy Sciences) in 0.2 M sodium carbonate-bicarbonate (“carb-bicarb”) buffer. After washes in 0.2 M carb-bicarb, flies were briefly dried and the lipophilic fluorescent dyes DiD (20 mg/mL in 100% ethanol, ThermoFisher, #D7757) and DiI (20 mg/mL in 1:1 dimethyl formamide:ethanol, ThermoFisher, #D3911) were applied to the exposed bristle sockets with glass micropipettes (Sutter Instruments, #BF100-50-10). Flies were incubated 48 hours in a humid chamber at room temperature, the ventral nerve cords (VNCs) were dissected in 0.2 M carb-bicarb buffer and filled mechanosensory axons were imaged on an LSM710 and LSM780 (Zeiss) confocal microscopes.

Labeling and analysis of growth cones of mechanosensory neurons during development

Genetic labeling of single pDc neurons was adapted from a genetic labeling strategy to investigate the developmental mechanism by which Wnk regulate axonal branch formation. Briefly, Flp-recombinase was expressed in precursors of pDc neurons using DC1.4 enhancer, which gives rise to stochastic expression. In this flp-out setups, pnr-gal4 activity was restricted

by using DC1.4-Flp to excise an FRT-flanked transcriptional STOP cassette from a UAS-mCD8::GFP reporter construct, whose expression is then trans-activated by pnr-Gal4. The defective branching pattern of adult pDc neurons with dWnk double RNAi knock-down is fully penetrant (n = 47). The phenotypic defect(s) of the adult mutant pDc axon projection is identical to single pDc axons of dWnk null mutant clones (generated by MARCM). White pupae were allowed to develop for various time intervals at 25°C until ~30 to 40 hr for wild-type and dWnk-knockdown. Dissected VNCs were stained with anti-GFP. Images were taken on a Zeiss LSM710 confocal microscope with a 60X lens. Filopodia were counted manually in Fiji / ImageJ in confocal microscopy image stacks of developing dWnk-knockdown and control animals with single mechanosensory neurons labeled with CD8::GFP.

Conditional knockdown of WNK

E15.5 embryos of time-pregnant F1 females from C57BL/6J x 120/SvJ were in utero electroporated with pCAG-ERT2CreERT2 (1 mg/mL) and a 1:1 ratio of either CreONWNK1-TRCN0000027035 and CreONWNK1-TRCN0000027039 or CreONWNK2-TRCN0000027661 and CreONWNK1-TRCN0000027668 (4 mg/mL). Activation of the ERT2CreERT2 fusion protein was achieved by intraperitoneal administration of tamoxifen for three consecutive days, starting at P30, (0.10 mg/g of bodyweight) dissolved in

corn oil (20 mg/mL) as previously described (Matsuda and Cepko, 2007). Corn oil alone was used as a vehicle control for littermates. Four days after the last injection i.e., 7 days following first injection (P37), mice were sacrificed via perfusion of 4% paraformaldehyde (PFA, Electron Microscopy Sciences) and 0.075% Glutaraldehyde (Electron Microscopy Sciences) followed by overnight post-fixation in 4% PFA/0.075% Glutaraldehyde.

Immunohistochemistry of Brain Slices

Post-fixed brains were sectioned via vibratome (Leica VT1200) at 110 μm. Floating sections were then incubated for 1 hour in 4% Normal Goat Serum, 2% BSA, 0.3% Triton X-100 in PBS to block non-specific binding. Primary and secondary antibodies were diluted as follows: chicken anti-GFP (5 μg/mL, Aves Lab-recognizes GFP and YFP; rabbit anti-RFP (1:1,000, Abcam–recognizes mTagBFP2, DsRED, and tdTomato); AlexaFluor goat anti-Chicken 488 (1:1000, Invitrogen); AlexaFluor goat anti-Rabbit 546 (1:1,000, Invitrogen). Floating sections were incubated overnight at 4°C in the primary antibodies, washed three times in PBS for 5 minutes each, then incubated in secondary antibodies for 5 hours at room temperature. Sections were mounted on slides and coverslipped with Fluoromount-G mounting medium (SouthernBiotech).

Immunolabelling

Cells were fixed for 5 min at room temperature in 4% (w/v) paraformaldehyde (Electron Microscopy Sciences) in PBS. Fixed cells were subsequently incubated in Permeabilisation Buffer (PB) (1x PBS supplemented with 0.1% Triton X-100 and 1% BSA (Sigma)) for 60 minutes to permeabilize and block non-specific staining. Primary antibodies were incubated for 1 hour at room temperature in PB, followed by an incubation with secondary antibodies for 30 min at room temperature in PB. Coverslips were mounted on slides with Vectashield mounting medium.

Drosophila single mechanosensory neuron labeling with axon and synaptic markers was done as described previously (Chen et al., 2006).

Mice were anaesthetized with isofluorane before intracardiac perfusion with 4% (w/v) paraformaldehyde in PBS followed by post-fixation in 4% PFA for 2 hours. 125 μm coronal brain sections were obtained using a vibrating microtome (Leica VT1200S). Sections were permeabilized 30 minutes in PB then incubated overnight with the indicated primary antibodies diluted in PB. Secondary antibodies were incubated for 1 hour at room temperature in PB. Slices were mounted on microscopy slides using Vectashield mounting medium.

Antibodies

The dWnk antibody was custom developed. For dWnk protein production in bacteria, PCR products of N-terminal and C-terminal fragments (as indicated in Figure S2) were amplified and cloned into pET vectors. Protein fragments expressed from these plasmids were tagged with 6xHis. Constructs were transformed into BL21DE3 competent cells (Agilent, #200131). Expression was induced in liquid LB medium cultures by adding IPTG (Sigma, #I6758-1G). Cells were grown for another 3 to 4 hours at 25°C and subsequently lysed in lysis buffer containing 50 mM Tris-HCl (pH 7.5), 150 mM NaCl and 2 mM DTT with sonication. His-tagged proteins in the lysate were purified by use of Ni-NTA agarose beads (QIAGEN, #30210) and washed in 30 mM imidazole in lysis buffer. Protein was eluted with 300 mM imidazole in lysis buffer. The eluate was further purified on an Amicon Ultra 0.5 mL 3K UFC column (#500396). Purified proteins were used for immunization of guinea pigs. Polyclonal antibody production was done by Covance (Denver, PA, USA). The dWnk antibody was used at a 1:300 dilution.

Other primary antibodies used in this study were: chicken anti-GFP (5 μg/mL, Aves Lab), mouse anti-SMI312R (1:1000, Covance), rabbit anti-MAP2 (1:1000, Millipore), rabbit anti-Cux1 (1:500, Santa Cruz), rat anti-HA high affinity (1:1000, Roche), rabbit anti-FLAG (1:2500, Sigma), mouse anti-V5 (1:1000, Sigma), rabbit anti-myc (1:1000, Abcam), rabbit anti-tubulin (1:1000, Novus Biologicals), rabbit anti-GFP (Invitrogen, 1:500), mouse anti-GFP (Abcam, 1:500), rabbit anti-DsRed (Takara Bio, 1:500), mouse anti-Fasciclin II (DSHB Hybridoma Product 1D4 anti-Fasciclin II, 1:20), and rat anti-N-Cadherin (DSHB Hybridoma Product DN-Ex #8, 1:20). Alexa-conjugated secondary antibodies (Invitrogen) were used at a 1:2000 dilution. HRP-conjugated secondary antibodies (Invitrogen or Jackson Laboratories) were used at a 1:10000 dilution. Nuclear DNA was stained using Hoechst 33258 (1:10000, Pierce).

Confocal image acquisition and analysis

Confocal images were acquired with a Nikon Ti-E microscope equipped with the A1 laser scanning confocal microscope using the Nikon software NIS-Elements (Nikon Corporation, Melville, NY). Dye-filled *Drosophila* axons were imaged using an LSM710 (Zeiss) confocal microscope. Analysis of confocal images was performed with NIS-Elements software or ImageJ.

Ilastik Cell Density Counter

The interactive density counter workflow from open-source software, Ilastik (Berg et al., 2019), was used to quantify the number of layer 2/3 PNs electroporated in each brain section quantified for axon optical density in Figures 4 and 6. This workflow is useful for identifying overlapping objects that classic segmentation and detection approaches cannot separate. The counter employs a supervised learning strategy guided by user annotations of background and object, which then serve as inputs into a Random Forrest regression that estimates every pixel's density. 10x confocal images from four different brain slices that spanned all time points were used for training the algorythm. Post processing of our Ilastik density outputs were performed in FIJI ImageJ. This included

binarizing and watershedding images. To count cells we employed FIJI's analyze particles function, excluding small objects and objects with low sphericity to remove objects corresponding to dendrite branches. To validate our Ilastik workflow we compared the cell count to manual counts performed by multiple observers (three). The number of cells per image estimated by Ilastik and Fiji pipeline lied within 10% of values obtained by human observers in a manner that was independent of density of electroporated neurons.

QUANTIFICATION AND STATISTICAL ANALYSIS

Data acquisition and quantification were performed non-blinded. Acquisition was performed in Microsoft Excel, statistical analyses were performed using Prism (GraphPad Software). Statistical details (definition of test, exact value of n (e.g., number of *Drosophila* VNCs, number of mouse brains, etc.), mean ± deviations, p values) are listed in Figure Legends and below.

Figure 3T: Ordinary one-way ANOVA with multiple Tukey's comparisons test, $n_{WT\text{-}early} = 16$; $n_{WnkKD\text{-}early} = 13$; $n_{WT\text{-}intermediate} = 17$; $n_{WnkKD\text{-}intermediate} = 12$; $n_{WT\text{-}late} = 14$; $n_{WnkKD\text{-}late} = 10$. The tests were considered significant when $p < 0.05$, with the following criteria: * $p < 0.05$, ** $p < 0.01$, *** $p < 0.001$, **** $p < 0.0001$.

Figures 4M–4P: Two-way ANOVA followed by multiple Tukey's comparisons test. Three sections from each brain were quantified, $n_{pLKO\ P10} = 3$; $n_{pLKO\ P15} = 3$; $n_{pLKO\ P21} = 5$; $n_{pLKO\ P35} = 5$; $n_{WNK1\ P10} = 4$; $n_{WNK1\ P15} = 3$; $n_{WNK1\ P21} = 3$; $n_{WNK1\ P35} = 5$; $n_{WNK2\ P10} = 3$; $n_{WNK2\ P15} = 3$; $n_{WNK2\ P21} = 4$; $n_{WNK2\ P35} = 3$. Statistical analysis: * $p < 0.05$, ** $p < 0.01$, *** $p < 0.001$, **** $p < 0.0001$.

Figures 5G–5J: Two-way ANOVA followed by multiple Tukey's comparisons test. Number of neurons for quantification: $n_{pLKO} = 19$, $n_{shWNK1} = 28$, $n_{shWNK2} = 23$ from at least three independent experiments. Significance: * $p < 0.05$ with the following criteria: * $p < 0.05$; ** $p < 0.01$; ***$p < 0.001$; ****$p < 0.0001$.

Figure 6: Mann-Whitney test (N and W) or a two-way ANOVA followed by Tukey's multiple comparisons test (M and V): * $p < 0.05$, ** $p < 0.01$, *** $p < 0.001$, **** $p < 0.0001$. Number of mice for each experimental condition: $n_{CreON\text{-}shWNK1\ +\ Vehicle} = 3$; $n_{CreON\text{-}shWNK1\ +\ Tamoxifen} = 3$; $n_{CreON\text{-}shWNK2\ +\ Vehicle} = 3$, $n_{CreON\text{-}shWNK2\ +\ Tamoxifen} = 4$. At least 3 sections analyzed per brain as described for Figure 4.